

9. FLUIDS IN OCEANIC LAYER 3: EVIDENCE FROM VEINED ROCKS, HOLE 735B, SOUTHWEST INDIAN RIDGE

David A. Vanko² and Debra S. Stakes³

ABSTRACT

Rock samples from Hole 735B, Southwest Indian Ridge, were examined to determine the principal vein-related types of alteration that occurred, the nature of fluids that were present, and the temperatures and pressures of these fluids. Samples studied included veined metagabbro, veined mylonitic metagabbro, felsic trondhjemite, and late-stage leucocratic diopside-bearing veins. The methods used were standard petrographic analysis, mineral chemical analysis by electron microprobe, fluid inclusion petrography and analysis by heating/freezing techniques and laser Raman microspectroscopy, and oxygen isotopic analyses of mineral separates.

Alteration in lithologic Units I and II (above the level of Core 118-735B-30R; approximately 140 meters below the seafloor) is dominated by hydration by seawater-derived fluids at high temperature, up to about 700°C, and low water/rock ratio, during and immediately after pervasive ductile deformation. Below Core 118-735B-30R, pervasive deformation is less common, and brittle veining and brecciation are the major alteration styles. Leucocratic centimeter-scale veins, often containing diopside and plagioclase, were produced by interaction of hot (about 500°C) seawater-derived fluid and gabbro. The water/rock ratio was locally high at the veins and breccia zones, but the integrated water/rock ratio for the lower part of the hole is probably low.

Accessory hydrous magmatic or deuteric phases formed from magmatic volatiles in some gabbro and in trondhjemite. Most subsequent alteration was affected by fluids that were seawater-derived, based on isotopic and chemical analyses of minerals and analyses of fluid inclusions. Many early-generation fluid inclusions, associated with high-temperature veining, contain appreciable methane as well as saline water. The source of methane is unclear, but it may have formed as seawater was reduced during low water/rock interaction with ultramafic upper mantle or ultramafic and mafic layer 3.

Temperatures of alteration were calculated on the basis of coexisting mineral chemistry and isotopic values. Hydrothermal metamorphism commenced at about 720°C and continued to about 550°C. Leucocratic veining took place at about 500°C. Alteration within brecciated horizons was also at about 500° to less than 400°C, and the trondhjemite was altered at about 550° to below 490°C. Pressures calculated from a diopside-bearing vein, based on a combination of fluid inclusion and isotopic analysis, were 90 to 100 MPa. This pressure places the sample, from Core 118-735B-70R in Unit V, at about 2 km below the seafloor.

INTRODUCTION

Information regarding the types and variety of fluids that may exist at various times within plutonic layer 3 of the ocean crust has been, until recently, limited to that obtained from reconnaissance studies of dredged or submersible-sampled rocks exposed on the seafloor by tectonic processes, and studies of ophiolites. Many plutonic oceanic rocks have interacted with seawater, resulting in observed shifts in stable isotope values of minerals (e.g., Stakes and O'Neil, 1982; Ito and Clayton, 1983) and resulting in fluids trapped as inclusions in hydrothermal minerals (Stakes and Vanko, 1986; Vanko, 1988). Some plutonic oceanic rocks also contain evidence for the presence of magmatic volatiles: in some studies (e.g., Prichard and Cann, 1982; Mevel, 1988) hydrous phases such as pargasitic amphibole are taken as evidence of a magmatic fluid component, and some fluid inclusions in magmatic phases in seafloor gabbros may be magmatic in origin (Kelley and Delaney, 1987). Ophiolite plutonic rocks contain oxygen isotopic evidence for exchange with seawater, sometimes through as much as 5 km of stratigraphic section (Gregory and Taylor, 1981; Harper et al., 1988).

Hole 735B, at the Atlantis II Fracture Zone along the Southwest Indian Ridge, provides a nearly continuous core (average recovery of 87%) through 500.7 m of oceanic plutonic rocks, many of which contain evidence for the former presence of fluids. Based on data reported here, the fluids were variable in temperature and in composition, ranging from early high-temperature fluids of both seawater and possible mantle origin, to low-temperature seawater-derived fluids.

The objective of this study is to document petrological data bearing on the variety of fluids that invaded layer 3 at Hole 735B and to evaluate their role in metamorphism and alteration. Our approach is to combine petrography with three complementary data sets: mineral chemistry determined by electron microprobe, fluid inclusion characteristics determined through heating and freezing and nondestructive laser Raman microprobe analyses, and oxygen isotopic determinations for mineral separates. We have examined more than 100 thin sections from Hole 735B samples, and have microprobed more than 30 of these in detail. Fluid inclusions in 10 samples have been analyzed by laser Raman microspectroscopy, and detailed heating and freezing data are available from six samples. The data reported are from four general lithologies encountered within the drillhole: veined metagabbro, mylonitized metagabbro, trondhjemite (or plagiogranite), and centimeter-scale leucocratic diopside-bearing veins.

Our results indicate that seawater, and perhaps mantle fluids, had a role in metamorphism and alteration of the plutonic rocks. The seawater-derived fluid produced abundant amphibole in veined metagabbros, particularly in the upper

¹ Von Herzen, R. P., Robinson, P. T., et al., 1991. *Proc. ODP, Sci. Results*, 118: College Station, TX (Ocean Drilling Program).

² Department of Geology, Georgia State Univ., Atlanta, GA 30303, U.S.A.

³ Department of Geology, Univ. of South Carolina, Columbia, SC 29208, U.S.A.

portions of the drill hole. A distinctive fluid, composed dominantly of water and methane, is present within some fluid inclusions in some veined metagabbros and in trondhjemite. We interpret this fluid as having derived from seawater, but we speculate about the origin of the methane and consider such sources as a mantle volatile reservoir, late magmatic volatiles, or generation of methane by hydration or serpentinization reactions in the underlying upper mantle or within layer 3 itself.

Geological Setting

Hole 735B was drilled near the Atlantis II Fracture Zone, a 210-km left-lateral transform offset of the Southwest Indian Ridge (Fig. 1). The hole was situated on a 700-m-deep wave-cut platform that formed the summit of an uplifted block, east of the active transform. This platform is one of a series of uplifted blocks that form a linear "transverse ridge" parallel to the transform. The platform is composed of massive gabbro covered by thin discontinuous sediment drift. Site 735B is about 93 km south of the present-day Southwest Indian Ridge axis where the crust originally formed approximately 11 Ma ago. It is more than 18 km from the axis of the transform fault (Dick et al., this volume), and foliation in the rocks strikes parallel to the spreading center. Thus, the plutonic crust here is interpreted to represent slow-spread igneous crust formed well away from the ridge-transform intersection (Dick et al., this volume).

Lithostratigraphy (Fig. 2) is entirely plutonic, and consists of gabbro and metagabbro modified locally by intense ductile deformation (to produce gneissic metagabbro and mylonite), brecciation (along discrete meter-scale horizons), centimeter-scale veining, and high-temperature "syntectonic late magmatic differentiation" (Dick et al. this volume). Approximately one-third of the core is essentially undeformed, with the rest exhibiting at least some deformation. For a complete lithostratigraphic description and geological overview, see Dick et al. and other papers in this volume.

ANALYTICAL METHODS

Mineral chemistry was determined using the Cameca SX-50 electron microprobe at the University of South Carolina. Calibration was accomplished using both mineral and pure compound standards, and mineral reference standards were analyzed to ensure that precision for major elements remained within 2 rel%, and for minor elements remained within 5 rel%. Mineral analyses that have been recalculated as

molar percent of some mineral component (e.g., An_{60}) are generally good to ± 1 mol%. However, for plagioclases, we found that sodium loss became significant for the more sodic varieties. Consequently, the anorthite contents reported are good to ± 1 mol% for labradorite analyses, to about ± 2 mol% for oligoclase and andesine analyses, and to about ± 4 mol% for albite analyses.

Fluid inclusions were observed using a USGS-type heating and freezing stage, where phase transition temperatures could be measured with a precision of $\pm 0.1^\circ\text{C}$ during freezing and $\pm 0.5^\circ\text{C}$ during heating. Accuracy of $\pm 0.2^\circ$ (freezing runs) and $\pm 1.0^\circ\text{C}$ (heating runs) was ensured by calibrating the thermocouple vs. known transitions at -56.6° , 0.0° , and $+374^\circ\text{C}$. Samples selected for fluid inclusion analyses were cut into doubly polished thin sections ranging from about 0.25 mm down to about 40 μm thick. Extremely thin doubly polished sections were necessary to view inclusions in plagioclase and amphibole. Selected fluid inclusions were analyzed by laser Raman microspectroscopy in the Vibrational Spectroscopy Laboratory at Virginia Polytechnic Institute and State University. Laser Raman spectra obtained for individual inclusions can detect the presence of Raman-active molecular species at levels of the order of 1 atm partial pressure (Wopenka and Pasteris, 1987). This probably corresponds to a detection limit of the order of 1 mol% in our inclusions. Species of interest that were sought in this study are CO_2 , CO_3^{2-} , CO , CH_4 , H_2 , H_2S , HS^- , SO_2 , SO_4^{2-} , N_2 , NH_3 , and graphite.

Oxygen was extracted from whole rock powders and from mineral separates by reaction with ClF_3 at temperatures of 550° to 650°C (modified from Clayton and Mayeda, 1963). Samples were dried for more than 1 hr in a 100°C oven before loading into the reaction vessels purged with dry argon. The oxygen was converted to CO_2 by reaction with a heated carbon rod prior to isotopic analyses. All isotopic analyses were performed on a VG 602 mass spectrometer in the Stable Isotope Laboratory of the University of South Carolina. Reproducibility was $\pm 0.3\%$ using Ottawa Sand and NBS-28 as standards. Replicate analyses were performed on all samples, and reported values are averages of these replicates. All results are presented in per mil notation standardized to Standard Mean Ocean Water. An increase in the per mil value represents a relative enrichment in the heavier isotope.

Three types of samples were analyzed for oxygen. A set of homogeneous powders was prepared on board the *JOIDES Resolution* for X-ray fluorescence analyses. Splits of these whole-rock powders were analyzed for oxygen isotopes to

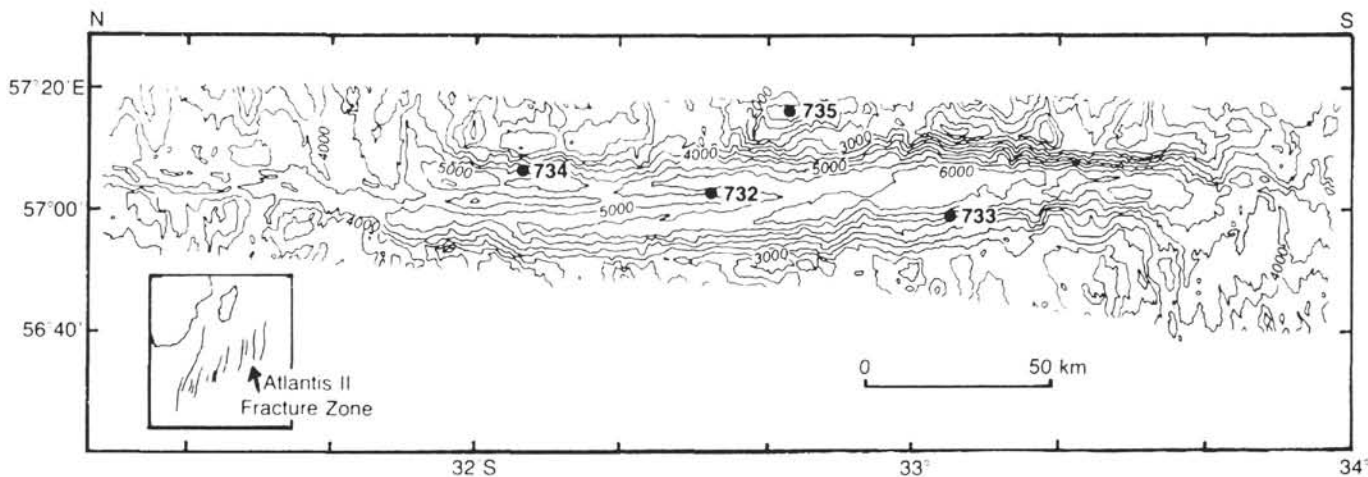


Figure 1. Location map for ODP Hole 735B, Southwest Indian Ridge.

Hole 735B Lithologic Variability

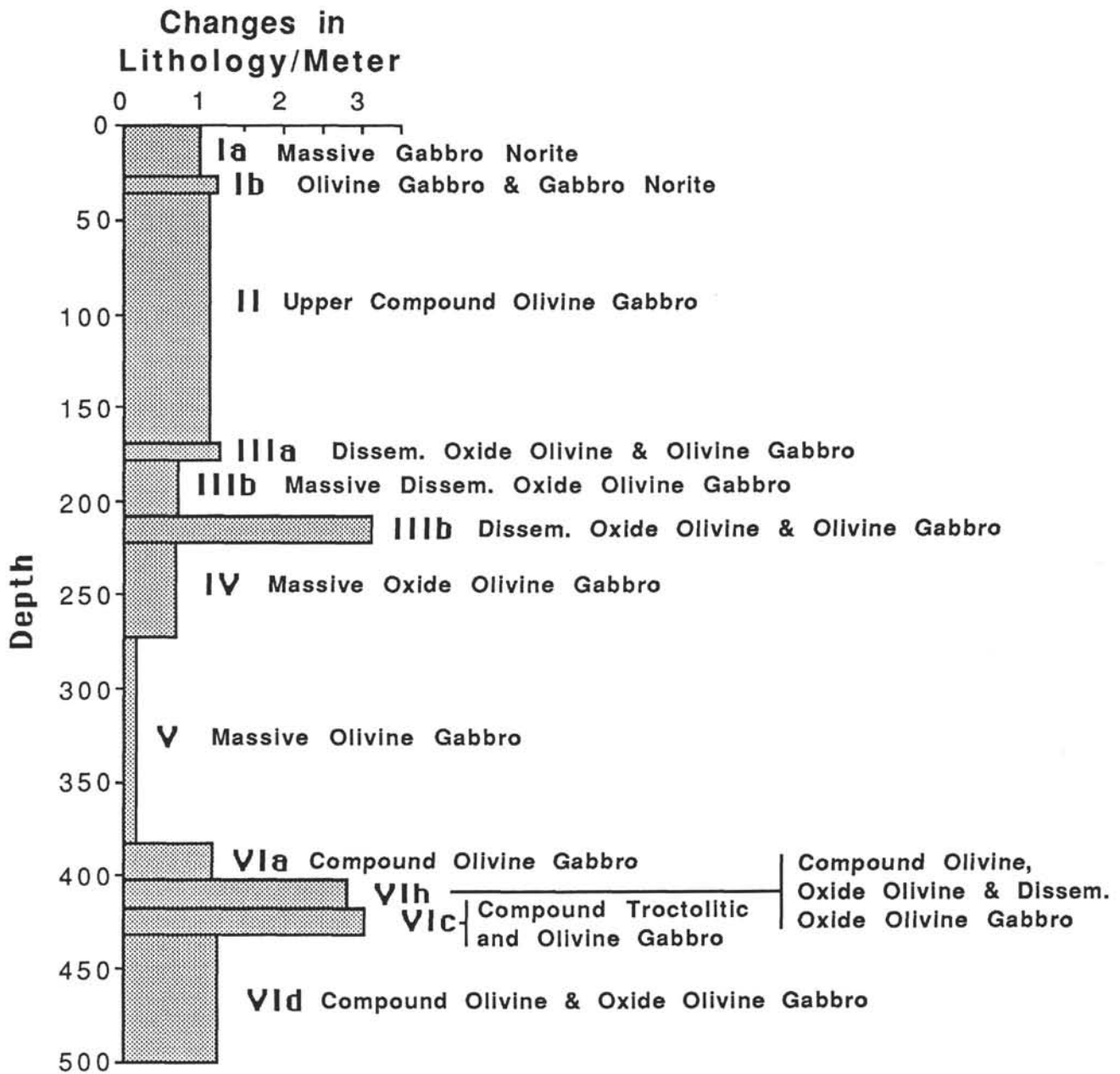


Figure 2. Schematic lithologic log for Hole 735B showing major lithologic changes, unit designations, and depths (from Dick et al., this volume).

Table 1. Summary of mineralogical data for some Hole 735B samples.

Lith unit	Sample	Type	Cum	Chl	Diop	Ap	Cc	Ep	Tt	Qtz	Mica	Zir	Other	Plag An %	Amph composition	Misc. data
IA	118-735B-1D-1 (Piece 1, 0–5 cm)	1,2												46; 20	Mg-hb; mg-hast-hb; act	
IA	118-735B-2D-2 (Piece 6, 36–39 cm)	1,3				Ap								55–50	Mg-hb; tsch-hb; mg-hast; act	
IA	118-735B-7D-1 (Piece 2A, 10–16 cm)	1,2	Cum	Chl										47–43; 31	Mg-hb; mg-hast-hb; act	Chl Fe# = 28
II	118-735B-12R-1 (Piece 5D, 65–68 cm)	1,4											Hematite	72–64; 31 Vein	Eden-hb; mg-hb; mg-hast-hb; act	
II	118-735B-14R-3 (Piece 2A, 31–35 cm)	1,2		Chl			Cc							50–48	Mg-hb	
II	118-735B-20R-2 (Piece 1B, 9–13 cm)	1,3												Mg-hb, tsch-hb		
II	118-735B-22R-3 (Piece 5A, 112–115 cm)	1,3	Cum	Chl										59–52; 30–28	Tsch-hb; mg-hb; act	Chl Fe# = 22
II	118-735B-25R-1 (Piece 3, 12–17 cm)	1											Ilm, pyr	65–61; 47–43; 26–24	Mg-hb; act-hb	
II	118-735B-26R-2 (Piece 2A, 8–12 cm)	1,3												62; 44–41 Vein	Mg-hb; act	
II	118-735B-35R-2 (Piece 4G, 102–106 cm)	1			Diop	Ap		Ep		Qtz	Mica	Zir		31; 22–20; 16; 5–2 (To 7% Or)	Act-hb; act	
IIIA	118-735B-35R-7 (Piece 2, 14–17 cm)	1			Diop						Mica		Talc	44–41	Parg, fe-parg, act, act-hb	Fo65–62
IIIA	118-735B-36R-1 (Piece 3, 17–20 cm)	1	Cum								Mica		Opaq	38–37	Mg-hb	
IIIA	118-735B-37R-2 (Piece 1H, 113–117 cm)	7,8	Cum	Chl		Ap		Ep					Anl	61–58; 37–34; 21; 15	Mg-hast-hb; eden-hb; mg-hb; act-hb; act	Ep = Ps17,12,6
IIIB	118-735B-38R-4 (Piece 7B, 140–143 cm)	1,5					Cc						Opaq			Calcite by XRD
IIIC	118-735B-45R-4 (Piece 7, 136–140 cm)	1,3	Cum	Chl	Diop	Ap			Tt		Mica		Opaq, anl, talc	63–62	Mg-hast; eden-hb; mg-hb; trem	Chl Fe# = 56,84; Ep = Ps17,14; phlogMg# = 75; 0.01 %Cl
IV	118-735B-53R-4 (Piece 1B, 5–15 cm)	9	Cum											32–29; 20–16	Mg-hb	
IV	118-735B-54R-2 (Piece 1C, 32–34 cm)	9				Ap				Qtz	Mica			32–30; 16, 10, 5	Fe-hb; fe-act-hb	Biot mg# = 20,21; 0.2–0.3 %Cl
V	118-735B-57R-2 (Piece 1B, 11–18 cm)	1													Mg-hb; act	
V	118-735B-58R-1 (Piece 10, 47–51 cm)	1		Chl				Ep	Tt				Preh, thom	63–56; 31, 25–22; 11, 10, 3	Tsch-hb; mg-hb; act-hb; trem	Chl Fe# = 34; Ep = Ps0,5
V	118-735B-58R-2 (Piece 1B, 10–17 cm)	1												52; 28; 1	Mg-hb; act-hb; trem	

Table 1 (continued).

Lith unit	Sample	Type	Cum	Chl	Diop	Ap	Cc	Ep	Tt	Qtz	Mica	Zir	Other	Plag An %	Amph composition	Misc. data
V	118-735B-63R-6 (Piece 5A, 94–98 cm)	1,6		Chl	Diop		Cc	Ep	Tt				Anl	64–54; 37, 32, 20		Chl Fe# = 37; Ep = Ps9
V	118-735B-65R-2 (Piece 1B, 18–25 cm)	1			Diop									65–53; 30	Eden-hb; mg-hb; act	
V	118-735B-68R-3 (Piece 5, 62–64 cm)	7,3		Chl	Diop		Cc	Ep	Tt					65–52; 20–18	Mg-hast; act-hb; trem	Ep = Ps12,17; fe-chl
V	118-735B-70R-1 (Piece 2B, 39–49 cm)	1,6		Chl	Diop		Cc	Ep	Tt				Preh	67–58; 15–9		Chl Fe# = 27–46; Ep = Ps6,10; pink titanite
V	118-735B-70R-2 (Piece 2, 8–10 cm)	1			Diop			Ep	Tt				TiO ₂	53; 44; 29		
V	118-735B-73R-6 (Piece 6C, 60–65 cm)	1													Tsch-hb; mg-hb; act-hb	
VIB	118-735B-78R-4 (Piece 5B, 54–59 cm)	1	Cum					Ep	Tt		Mica		Talc	66; 17	Tsch-hb; act	Biot-0.4 %Cl
VID	118-735B-81R-2 (Piece 1C, 23–31 cm)	1,10				Ap			Tt	Qtz		Zir		59–56; 33–30; 12; 3–1	Act; fe-act	
VID	118-735B-85R-4 (Piece 1C, 17–25 cm)	1												55; 17–15	Fe-parg-hb; act	
VID	118-735B-87R-5 (Piece 3, 20–22 cm)	1,4	Cum											45–37	Act; fe-act	
VID	118-735B-87R-7 (Piece 1C, 15–17 cm)	11		Chl	Diop	Ap	Cc							26–22; 14	Eden	Fe-chl

Rock types: 1 = metagabbro; 2 = foliated, 3 = veined; 4 = mylonitic; 5 = calcite vein; 6 = cm-scale diopside-bearing vein; 7 = gabbro; 8 = brecciated; 9 = trondhjemite; 10 = cm-scale leucocratic vein; 11 = "autobreccia."

Mineral abbreviations: cum = cummingtonite; chl = chlorite; diop = diopside; ap = apatite; cc = calcite; ep = epidote; tt = titanite (sphene); qtz = quartz; zir = zircon; ilm = ilmenite; pyr = pyrite; opa = opaque; anl = analcime; preh = prehnite; thom = thomsonite; mg-hb = magnesiohornblende; mg-hast-hb = magnesio-hastingsitic hornblende; act = actinolite; tsch-hb = tschermakitic hornblende; mg-hast = magnesiohastingsite; eden-hb = edenitic hornblende; parg = pargasite; fe-parg = ferropargasite; trem = tremolite; fo = forsterite; biot = biotite.

produce the downcore profile discussed in Stakes et al. (this volume). In the upper portion of the core, these XRF powders were taken to represent evenly both altered and fresh portions of the core. Sampling from the lower portion of the core (during increasing time constraints) primarily reflects parts of the core that appeared the least altered. Bulk rock powders from additional samples were prepared, especially to supplement the XRF powders taken from the lower half of the core. Those designated "bulk" are a representative powder of what is usually a coarsely heterogeneous altered rock. These samples include heavily fractured and veined material. Samples designated "matrix" signify altered host rock from which a vein, feldspathic intrusion, or heavily altered shear zone was removed.

Silicate phases were separated by a combination of physical methods, including magnetic separation. Data presented here for veins are preliminary, as this work is still in progress. Large veins were separated from the host rock, crushed separately, and component phases were hand-picked. Plagioclase separates were X-rayed for purity, as veinlets of analcime, carbonate, or thomsonite are common replacements. Mineral separates were cleaned with acetone and dried in an oven for at least 2 hr prior to loading to minimize adsorbed water.

RESULTS

General Petrography

Several rock types described by the Leg 118 shipboard scientists have interacted to some degree with crustal fluids (Shipboard Scientific Party, 1989). This is particularly true for the plastically deformed rocks, which were classified using the following scheme on the ship: (1) poorly foliated gabbro, (2) foliated gabbro, (3) porphyroclastic gabbro, (4) augen gneissic gabbro, and (5) mylonitic gabbro. Additional types of metamorphosed or "altered" rock that provide evidence for fluids in the crust include brecciated gabbro, silicic intrusive material classified as trondhjemite, and leucocratic calc-silicate veins, commonly about 1 cm wide, characterized by a diopside-bearing assemblage. Many of the fresh gabbros in Hole 735B may never have been influenced by a fluid, although in these gabbros small amounts of brown amphibole have been reported as ubiquitous (Shipboard Scientific Party, 1989, p. 126). This amphibole is probably late magmatic in origin, signifying increased water fugacity in the melt at the last stage of crystallization, and does not necessarily indicate the presence of a discrete fluid phase.

In general, altered rocks from Hole 735B demonstrate a correlation between the degree of deformation and the proportion of hydrated phases. Such a relationship has been shown previously to apply to dredged oceanic plutonics (Malcolm, 1981; Vanko and Batiza, 1982; Ito and Anderson, 1983; Batiza and Vanko, 1985), and has been assumed to indicate that hydration reactions are concentrated near zones of deformation, which provide the pathways for lower crustal hydrothermal flow. Exceptions to this correlation between deformation and hydration are some mylonitic gabbros that were initially deformed at temperatures above amphibole stability limits (Stakes et al., this volume).

The upper 37.5 m of Hole 735B (Unit I) comprises a foliated metagabbro that is both plastically deformed and altered/metamorphosed (unit boundaries are those of Dick et al., this volume). Unit II (37.5–170.2 m below the seafloor [mbsf]) comprises olivine gabbros that exhibit much less plastic deformation and, consequently, a much lower degree of alteration. The freshest and essentially undeformed gabbros contain only a trace of brown amphibole of probable magmatic origin. Altered gab-

bro in Unit II correspond to a few zones of plastic deformation and to a brecciated horizon near the base of the unit.

Unit III (170.2–223.6 mbsf) is an olivine gabbro intercalated with thin units of iron-titanium oxide gabbro. Its upper boundary is a chemical one, gradational to the gabbros of Unit II. The lower boundary of Unit III is a sheared contact. Plastic deformation in Unit III is limited to zones between 180 and 200 mbsf. Unit IV (223.6–274.1 mbsf) is an iron-titanium oxide gabbro bounded on top and bottom by shear or fault zones. Plastically deformed zones within Unit IV are common from 250 to 274 mbsf.

Units V (274.1–382.4 mbsf) and VI (382.4–500.7 mbsf) are olivine gabbro and olivine-rich gabbro or troctolite, respectively. Plastic deformation is rare in Unit V, but common in Unit VI.

Superimposed on the early plastic deformation features within each lithologic unit are veins of varying types (see Dick et al., this volume, for downhole logs of vein types and their dips). Generally ranging from 1 mm to 1 cm wide, the veins are primarily filled by amphibole and plagioclase-amphibole. These veins typically occur nearly perpendicular to foliation, where present, suggesting that they are brittle features formed in the same stress field that caused the foliation (Shipboard Scientific Party, 1989, p. 105). Shipboard counts of vein density reveal up to 11 veins per meter of core, and few cores exhibit no veining (Stakes et al., this volume). Veins related to plastic deformation are least common in the gabbros of Unit V and are particularly abundant in gabbros of Units II and III.

A second vein type that occurs within Units II (near its base), III, V, and VI, is centimeter-scale, leucocratic, diopside-bearing veins. These are steeply dipping, usually about 1 cm wide, and may have a centimeter-scale leucocratic alteration halo in the host gabbro. Minerals filling the veins include plagioclase, diopside, and amphibole. Titanite, apatite, prehnite, and calcite are typical accessories.

Seven zones (three major ones) of brecciation occur within Units IV, V, VI, and at the base of Unit II. Breccias are cemented by a felsic assemblage of plagioclase, amphibole, and accessories such as chlorite, diopside, epidote, prehnite, calcite, titanite, apatite, thomsonite, and analcime. Leucocratic diopside-bearing veins are more likely to occur above or below breccia zones (Stakes et al., this volume), and may have formed in response to tensile stresses within blocks of crust separated by low-angle fault zones.

Late-stage carbonate veins occur within Units II, III, and particularly Unit V. Calcite occurs as drusy and sparry crystalline material cementing tiny grains and rock fragments derived from the vein walls.

Examples of veined, brecciated, and intruded (in the case of trondhjemite) rocks were selected for detailed study. Next, we describe the petrography of these representative rock types. (A summary of petrographic data is provided in Table 1, and sample descriptions are in the Appendix.) We then present data about mineral chemistry, fluid inclusions, and stable isotopes and discuss how these data bear on defining the fluid types and conditions of rock-fluid interaction that have affected Hole 735B.

Veined Metagabbro and Veined Mylonite

Veined metagabbro refers to those gabbros that have been deformed in a ductile style to produce foliated metagabbros and gneisses, and are cross-cut by networks of amphibole and plagioclase-amphibole veins. They are characterized by variable amounts of hydrous minerals modifying the original anhydrous (or nearly so) magmatic assemblage. The modal proportions of alteration phases are directly related to the extent of deformation of the host gabbro: progressive plastic

or brittle deformation results in larger amounts of new plagioclase, amphibole, phyllosilicates, and accessory minerals. Veined metagabbro is abundant in lithologic Unit I, the top half of Unit II, and Unit VI. Lesser amounts of veined metagabbro, in intervals of the order of meters and less, occur in all of the lithologic units. Dick et al. (this volume) present logs of vein types, deformation intensity, and vein attitude, produced during a detailed study of all Hole 735B core at the core repository.

Typically, metagabbros have primary gabbroic texture consisting of labradorite laths, intergranular to poikilitic augite, and granular olivine. Depending on location within the section, the gabbro is deformed and exhibits foliation, cataclasis and variable degrees of grain size reduction. Much of the plagioclase may be totally recrystallized to an intermediate composition, and much of the pyroxene may be altered to amphibole. Sometimes, hydration coronas of tremolite, cummingtonite, and actinolite form around pyroxenes, and olivine is pseudomorphed by serpentine and opaques.

Networks of millimeter-scale green amphibole and plagioclase-amphibole veinlets crosscut the foliation orthogonally or at high angle (Fig. 3). In some samples, veinlets are vuggy, and amphibole that abuts the open pore spaces may exhibit dramatic oscillatory zonation, probably formed as fluid parameters fluctuated with time (Fig. 4). The vein amphiboles vary from magnesio-hornblende through actinolitic hornblende and, less frequently, actinolite. Amphiboles also replace pyroxene in the host rocks, and these are usually magnesio-hornblendes identical to that within the veins.

Igneous plagioclase (labradorite) is often fractured and veined by andesine or oligoclase (Fig. 5) in the vicinity of amphibole and plagioclase-amphibole veins. This secondary plagioclase contains fluid inclusions that must have been trapped during the alteration event, because the primary

igneous plagioclase contains significantly fewer, more rare, inclusions (Figs. 6, 7, 8).

Veined mylonitic gabbros occur primarily in Units I, II, and near the base of Unit IV. Sporadic mylonites are present in Unit III, and they are rare in Units V and VI (Dick et al., this volume). Some mylonites are strongly hydrated, with plagioclase and amphibole forming the foliation, and clinopyroxene present as relict porphyroclasts. Other mylonites are relatively anhydrous, and may have deformed at temperatures above amphibole stability limits (Stakes et al., this volume). Both types of mylonite may exhibit later cross-cutting amphibole vein networks, with the veins being nearly orthogonal to the mylonitic foliation.

Trondhjemite

Small trondhjemite intrusions occur in Units II, III, IV, and VI, and are rare in Units I and V. This distribution may be related to the occurrence of oxide-rich gabbros concentrated in Units III and IV and the absence of abundant oxide-rich gabbro in Units I and V, because the trondhjemite and iron-titanium-rich liquid may have formed as immiscible liquids (Dick et al., Natland et al., this volume). Regardless of the petrogenesis of the trondhjemite, it forms intrusive layers and veins that may contain inclusions of gabbroic wallrock. Primary minerals in the trondhjemite include blocky plagioclase tablets (oligoclase to albite) and quartz, with accessory biotite, apatite, and pyrite. Plagioclase and quartz form granophyric intergrowths (Fig. 9). The primary plagioclase and quartz also contain fluid inclusions (Fig. 10). Wallrock inclusions consist of andesine crystals cross-cut by oligoclase and albite veinlets, augite with amphibole alteration at the edge, and mafic clots containing concentrically-zoned hydrous phases (mica, cummingtonite, ferro-hornblende, ferro-actinolite). Trondhjemites may be cut by green amphibole veins.

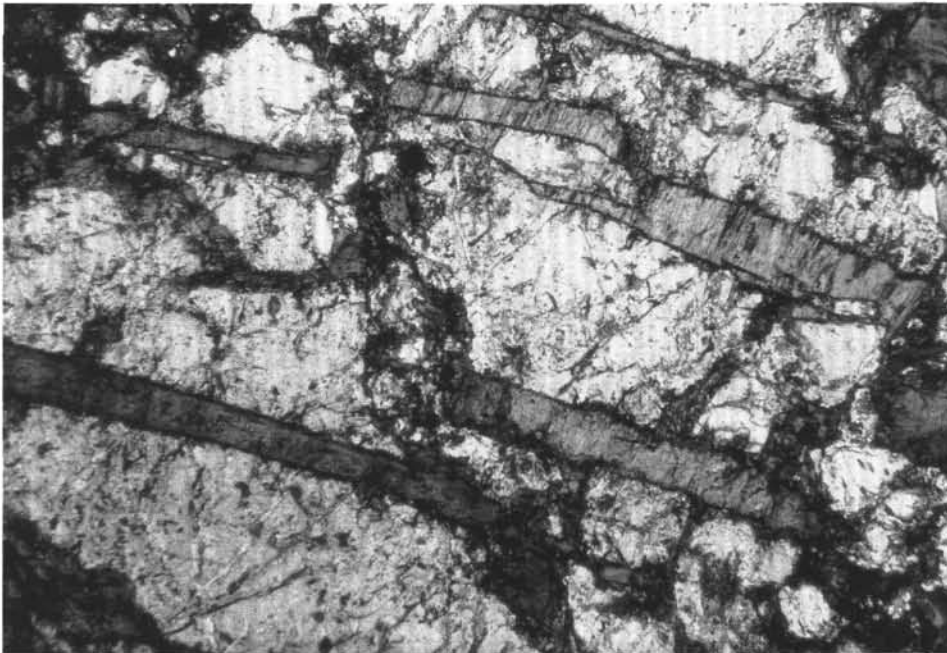


Figure 3. Photomicrograph of veined gabbro (Sample 118-735B-25R-1 [Piece 3, 12–17 cm]). Field of view is 2.5 mm wide. Hornblende in small veins has a cross-fiber texture. Note late-stage fracture offsetting the veins.

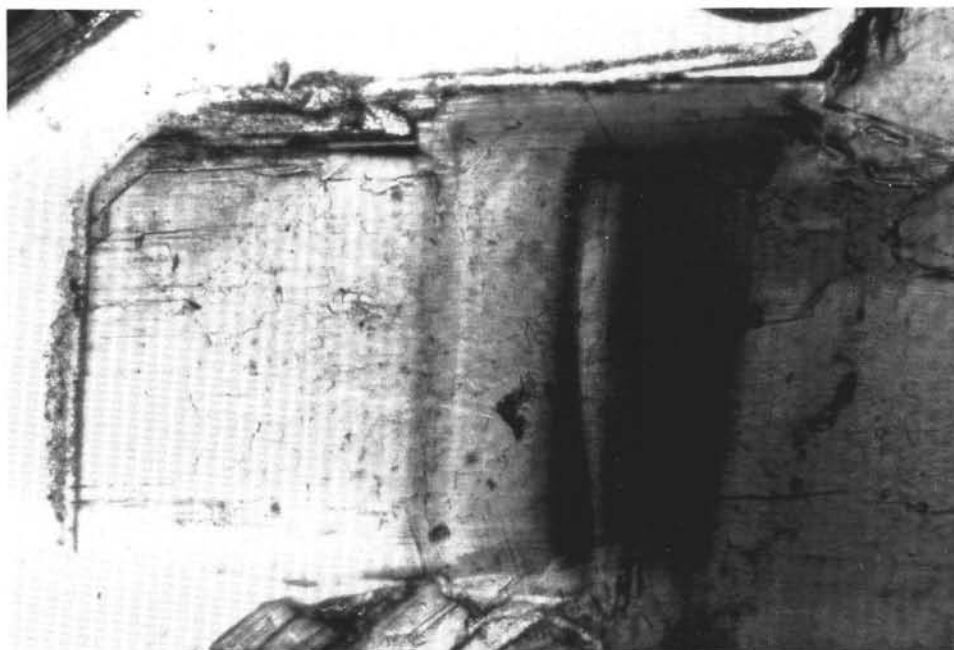


Figure 4. Photomicrograph of oscillatory zonation in hornblende, Sample 118-735B-26R-2 (Piece 2A, 8–12 cm). Dark amphibole to the right is magnesian hornblende, and clear amphibole to the left is actinolite (analyses in Table 2). Field of view is 0.65 mm wide.

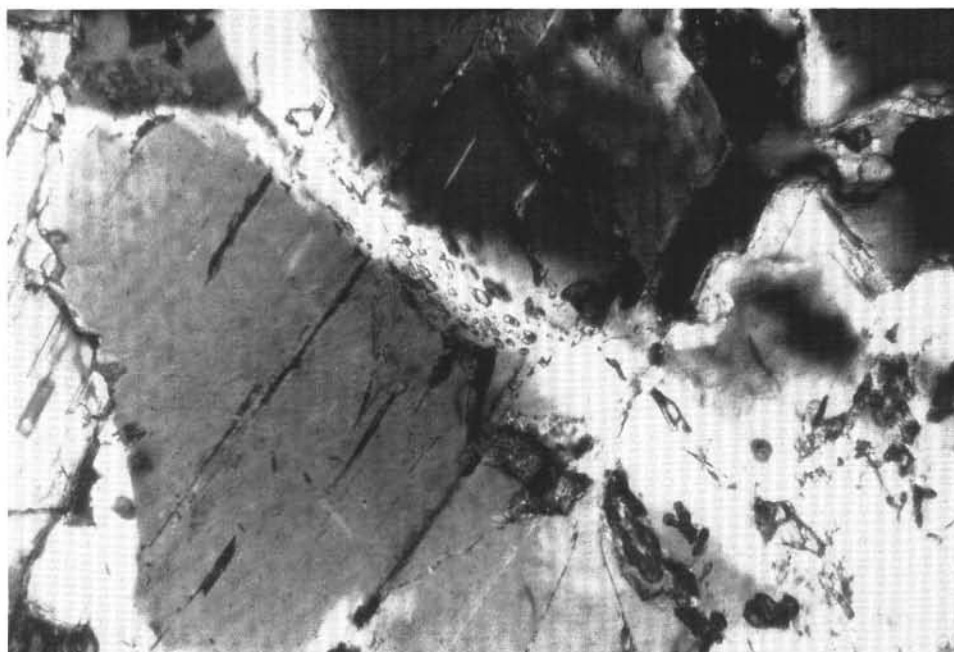


Figure 5. Photomicrograph of plagioclase veinlet (An₄₂) that crosscuts igneous labradorite (An₆₂) in metagabbro, Sample 118-735B-26R-2 (Piece 2A, 8–12 cm). Field of view is 0.65 mm wide.

Leucocratic Diopside-Bearing Veins

Below about 160 mbsf in Hole 735B, leucocratic centimeter-scale veins bearing sodic plagioclase and diopside were observed. These veins cut gabbros of lithologic Units II, III, V, and VI with steep dips ($60^\circ \pm 30^\circ$; Dick et al., this volume). They are notably absent in Unit IV and above the base of Unit II. They vary in color index (volume proportion of dark

phases) from near zero to about 50, and also vary in the sharpness of their borders with the host gabbros. Most leucocratic veins contain abundant fluid inclusions both in plagioclase and in diopside (Fig. 11).

Most commonly, veins have sharp parallel boundaries about 1 cm apart, and contain plagioclase (oligoclase to albite), diopside up to 50 vol%, and accessory pink titanite, clinzoisite, and chlorite. The host gabbros are labradorite-

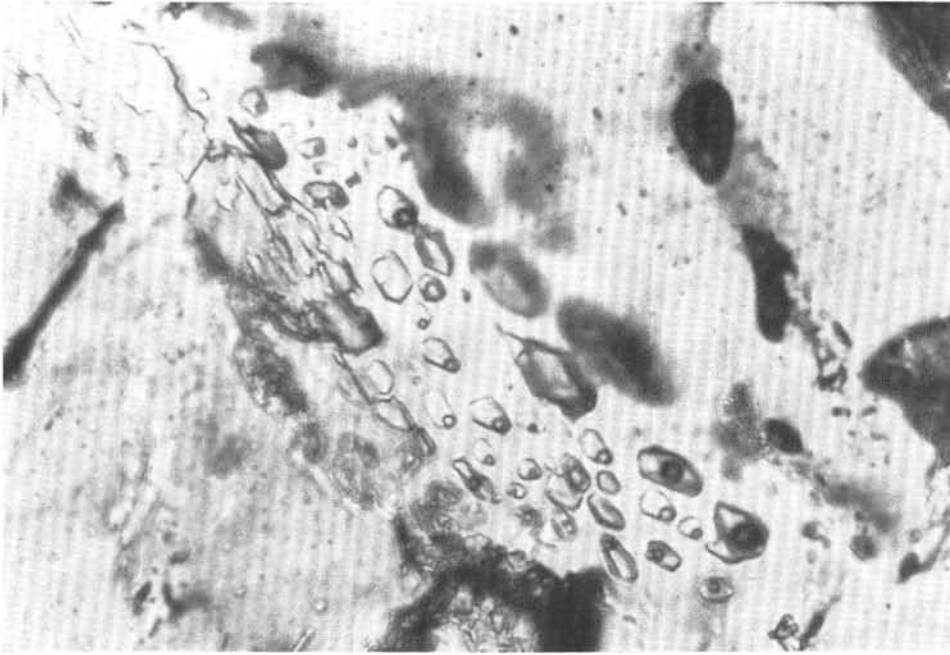


Figure 6. Close-up photomicrograph of fluid inclusions within andesine (An_{42}) veinlet from Figure 5. Field of view is 0.17 mm wide.

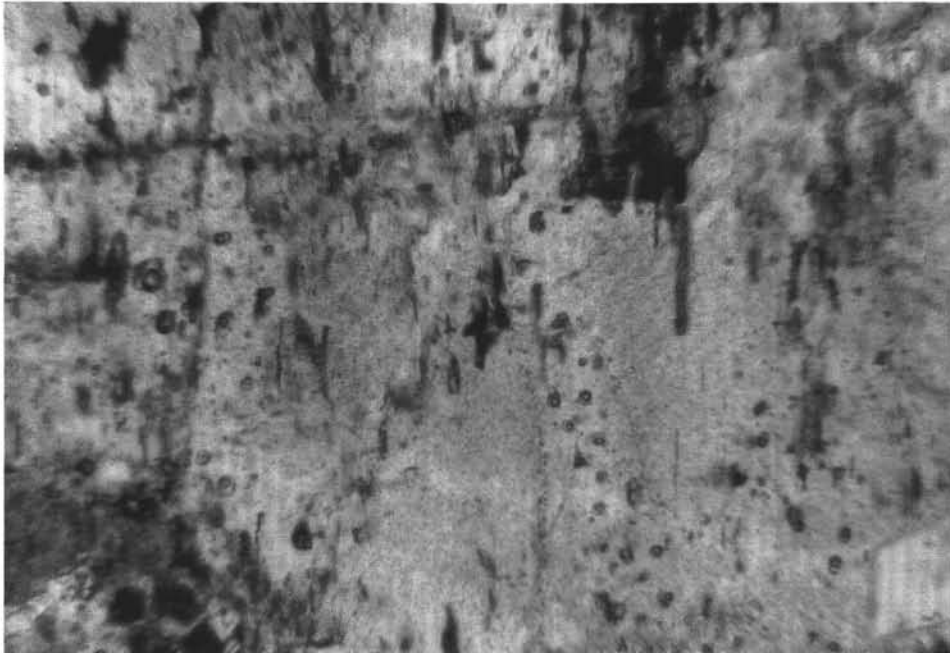


Figure 7. Photomicrograph of plagioclase in metagabbro, Sample 118-735B-58R-1 (Piece 10, 47–51 cm). Note that igneous labradorite is packed with tiny dark solid inclusions, whereas diffuse zones of secondary plagioclase (An_{31}) contain fluid inclusions and are devoid of solid black inclusions. Field of view is 0.65 mm wide.

augite and may also contain olivine or its hydrated pseudomorphs. The texture within the veins mimics the host gabbroic texture, as diopside appears to have grown epitaxially on the host wallrock augite during vein dilation (Fig. 12).

Some diopside-bearing veins have more gradational boundaries, and some leucocratic veins contain no diopside. Instead, the calc-silicate mineral is actinolite or ferro-actinolite,

and accessories include apatite, ilmenite, pink titanite, zircon, and rare quartz.

Mineral Chemistry

In this section, we present chemical analyses for most major hydrothermal mineral types and point out their significance in terms of the types and physical-chemical conditions of fluids that

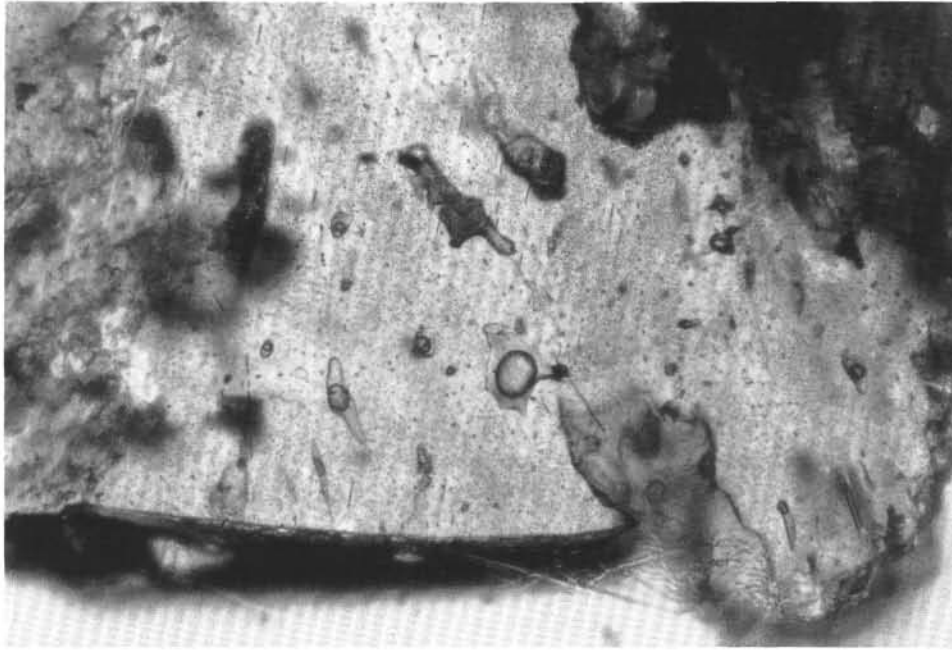


Figure 8. Photomicrograph of large fluid inclusions in plagioclase in metagabbro, Sample 118-735B-58R-1 (Piece 10, 47–51 cm). Field of view is 0.65 mm wide. The large inclusion with very large vapor bubble is 80 μm across. In addition to water and methane, this inclusion contains a small black hexagonal daughter crystal (in the extension to the right).



Figure 9. Photomicrograph of graphic or granophyric texture in the trondhjemite, Sample 118-735B-54R-2 (Piece 1C, 32–34 cm). Field of view is 4.8 mm wide.

were once present. Minerals not analyzed, but confirmed using EDS x-ray spectra, are titanite, ilmenite, pyrite, and zircon. A summary of our electron microprobe data is given in Table 1.

Amphiboles

Amphiboles are the most abundant secondary phases in Hole 735B. Representative amphibole analyses are listed in

Table 2. Good analyses total between about 96 and 99 wt%, because water is not analyzed or included in the table. Most amphiboles in Hole 735B are hornblendes of various subtypes; other common amphiboles are actinolite, tremolite, and cummingtonite.

The electron microprobe fails to differentiate ferric and ferrous iron, but analyses were recalculated using an algo-

Table 2. Representative amphibole analyses, Hole 735B samples.

Sample number:	118-735B-1D-1 (Piece 1, 0–5 cm)			118-735B-2D-2 (Piece 6, 36–39 cm)					118-735B-7D-1 (Piece 2A, 10–16 cm)					
	Mg-hb avg of 2 w/An ₂₀	Mg-hast-hb w/An ₄₆	Act	Mg-hb avg of 6 (vein)	Mg-hast avg of 7 (in cpx)	Actin	Mg-cumm avg of 2 (in coronas on cpx)	Tscher avg of 3	Mg-hst-hb avg of 2	Mg-hb vein	Mg-hb vein	Mg-hb vein	Mg-hb vein	Act avg of 3
SiO ₂	49.57	43.08	54.35	44.63	41.78	54.10	53.38	38.18	42.22	45.18	48.01	48.99	48.19	53.15
TiO ₂	0.60	1.66	0.21	0.55	2.99	0.10	0.01	0.00	1.58	0.38	0.27	0.39	0.46	0.16
Al ₂ O ₃	5.27	10.96	1.16	10.37	11.67	1.23	0.79	17.87	11.95	8.49	6.69	5.35	6.48	2.54
FeO*	13.18	17.45	12.25	14.10	11.93	9.06	18.35	14.00	14.19	17.40	15.09	14.04	14.28	13.99
MnO	0.16	0.19	0.11	0.19	0.16	0.23	0.95	0.20	0.21	0.24	0.28	0.27	0.33	0.47
MgO	15.45	10.82	16.90	13.09	13.20	18.69	20.92	12.07	12.17	12.27	14.39	14.98	14.82	18.21
CaO	12.48	11.85	12.78	11.35	11.65	12.53	1.52	10.99	11.44	11.27	11.11	11.49	11.14	9.00
Na ₂ O	1.24	2.54	0.32	2.06	2.46	0.28	0.20	3.03	2.93	2.17	1.68	1.47	1.71	0.73
K ₂ O	0.06	0.28	0.02	0.23	0.27	0.02	0.01	0.22	0.29	0.20	0.10	0.09	0.07	0.03
Cl	0.05	0.60	0.00	0.48	0.05	0.02	0.00	0.17	0.01	0.96	0.47	0.41	0.09	0.09
Total	98.04	99.43	98.10	97.03	96.17	96.26	96.11	96.74	96.97	98.56	98.09	97.48	97.57	98.37
O = Cl	0.01	0.14	0.00	0.11	0.01	0.00	0.00	0.04	0.00	0.22	0.11	0.09	0.02	0.02
Total	98.03	99.29	98.10	96.93	96.16	96.26	96.11	96.70	96.97	98.34	97.98	97.39	97.55	98.35
Routine	13ECNK	13ECNK	15ENK	13ECNK	13ECNK	15ENK	15ENK	15ENK	13ECNK	13ECNK	13ECNK	13ECNK	13ECNK	15ENK
Si	7.13	6.35	7.76	6.54	6.20	7.75	7.75	5.68	6.26	6.64	6.90	7.09	6.92	7.58
Al	0.87	1.65	0.24	1.46	1.80	0.25	0.25	2.32	1.74	1.37	1.10	0.92	1.08	0.42
Sum in T	8.00	8.00	8.00	8.00	8.00	8.00	8.00	8.00	8.00	8.00	8.00	8.00	8.00	8.00
Al	0.02	0.26	-0.05	0.33	0.24	-0.04	-0.11	0.81	0.35	0.11	0.04	0.00	0.02	0.01
Fe ³⁺	0.52	0.49	0.15	0.82	0.42	0.18	0.30	0.60	0.51	0.97	1.09	0.84	1.04	0.17
Ti	0.06	0.18	0.02	0.06	0.33	0.01	0.00	0.00	0.17	0.04	0.03	0.04	0.05	0.02
Mg	3.31	2.38	3.60	2.86	2.92	3.99	4.53	2.67	2.69	2.69	3.08	3.23	3.17	3.87
Fe ²⁺	1.06	1.66	1.28	0.91	1.06	0.85	0.28	0.92	1.25	1.16	0.73	0.86	0.68	0.94
Mn	0.02	0.02	0.00	0.02	0.02	0.00	0.00	0.00	0.03	0.03	0.03	0.03	0.04	0.00
Ca	0.00	0.00	0.00	0.00	0.00	0.00	0.00	0.00	0.00	0.00	0.00	0.00	0.00	0.00
Sum in C	5.00	5.00	5.00	5.00	5.00	5.00	5.00	5.00	5.00	5.00	5.00	5.00	5.00	5.00
Fe ²⁺	0.00	0.00	0.03	0.00	0.00	0.05	1.65	0.22	0.00	0.00	0.00	0.00	0.00	0.57
Mn	0.00	0.00	0.01	0.00	0.00	0.03	0.12	0.03	0.00	0.00	0.00	0.00	0.00	0.06
Ca	1.92	1.87	1.95	1.78	1.85	1.92	0.24	1.75	1.82	1.77	1.71	1.78	1.72	1.37
Na	0.08	0.13	0.00	0.22	0.15	0.00	0.00	0.00	0.18	0.23	0.29	0.22	0.29	0.00
Sum in B	2.00	2.00	2.00	2.00	2.00	2.00	2.00	2.00	2.00	2.00	2.00	2.00	2.00	2.00
Ca	0.00	0.00	0.00	0.00	0.00	0.00	0.00	0.00	0.00	0.00	0.00	0.00	0.00	0.00
Na	0.27	0.60	0.09	0.37	0.56	0.08	0.06	0.87	0.66	0.39	0.18	0.19	0.19	0.20
K	0.01	0.05	0.00	0.04	0.05	0.00	0.00	0.04	0.05	0.04	0.02	0.02	0.01	0.01
Sum in A	0.28	0.65	0.09	0.41	0.61	0.08	0.06	0.92	0.71	0.43	0.20	0.21	0.20	0.21
Cl	0.01	0.15	0.00	0.12	0.01	0.01	0.00	0.04	0.00	0.24	0.12	0.10	0.02	0.02
Mg#	75.69	58.88	73.31	75.93	73.54	81.58	70.16	69.88	68.22	69.76	80.97	79.05	82.37	72.36

Table 2 (continued).

Sample number:	118-735B-7D-1 (Piece 2A, 10-16 cm)	118-735B-12R-1 (Piece 5D, 65-68 cm)				118-735B-14R-3 (Piece 2A, 31- 35 cm)		118-735B-20R-1 (Piece 1B, 9-13 cm)		118-735B-22R-3 (Piece 5A, 112-115 cm)			
	Cumm	Ed-hb avg of 2 vein	Mg-hst- hb avg of 3 non-vein	Mg-hb vein	Act	Mg-hb avg of 11 vein = non-vein	St dev	Mg-hb	Tsch-hb	Tsch-hb	Mg-hb avg of 4	Act	Mg-cumm avg of 2
SiO ₂	52.64	43.46	43.30	46.63	52.81	46.56	0.94	45.90	42.60	44.18	47.56	51.82	53.07
TiO ₂	0.07	0.47	1.86	0.48	0.29	0.79	0.17	0.34	1.18	0.19	0.04	0.10	0.00
Al ₂ O ₃	2.29	9.14	9.71	6.69	2.53	7.84	0.73	8.08	12.56	13.26	8.91	3.67	2.04
FeO*	19.51	19.91	16.50	16.32	12.21	13.73	0.30	19.92	14.82	8.86	10.63	15.45	16.84
MnO	0.71	0.21	0.24	0.26	0.18	0.21	0.04	0.23	0.19	0.13	0.20	0.27	0.80
MgO	20.89	10.14	12.02	12.82	16.87	14.57	0.42	9.93	12.04	16.12	16.30	13.35	21.03
CaO	0.73	11.64	11.33	11.74	12.71	11.67	0.13	11.55	10.95	11.22	11.46	12.63	2.57
Na ₂ O	0.20	2.21	2.44	1.68	0.63	1.92	0.14	1.59	2.60	2.71	1.88	0.35	0.15
K ₂ O	0.30	0.34	0.28	0.22	0.07	0.19	0.04	0.11	0.18	0.18	0.12	0.03	0.00
Cl	0.01	1.44	0.53	0.69	0.06	0.31	0.04	0.23	0.05	0.01	0.16	0.00	0.00
Total	97.35	98.94	98.20	97.53	98.36	97.78	0.75	97.88	97.17	96.86	97.25	97.67	96.48
O = Cl	0.00	0.33	0.12	0.16	0.01	0.07	0.01	0.05	0.01	0.00	0.04	0.00	0.00
Total	97.35	98.61	98.08	97.37	98.35	97.71	0.75	97.83	97.16	96.86	97.21	97.67	96.48
Routine	15ENK	13ECNK	13ECNK	13ECNK	15ENK	13ECNK		13ECNK	13ECNK	13ECNK	13ECNK	13ECNK	15ENK
Si	7.58	6.53	6.39	6.90	7.53	6.74	0.08	6.83	6.24	6.28	6.80	7.55	7.63
Al	0.42	1.47	1.61	1.10	0.47	1.26	0.08	1.17	1.76	1.72	1.20	0.45	0.37
Sum in T	8.00	8.00	8.00	8.00	8.00	8.00	8.00	8.00	8.00	8.00	8.00	8.00	8.00
Al	-0.04	0.15	0.08	0.07	-0.04	0.08	0.07	0.25	0.41	0.50	0.31	0.18	-0.02
Fe ³⁺	0.33	0.76	0.78	0.68	0.26	0.81	0.09	0.68	0.89	0.99	0.66	0.21	0.35
Ti	0.01	0.05	0.21	0.05	0.03	0.09	0.02	0.04	0.13	0.02	0.00	0.01	0.00
Mg	4.48	2.27	2.64	2.83	3.59	3.14	0.08	2.20	2.63	3.41	3.48	2.90	4.51
Fe ²⁺	0.21	1.74	1.26	1.34	1.17	0.85	0.11	1.80	0.92	0.06	0.54	1.67	0.16
Mn	0.00	0.03	0.03	0.03	0.00	0.03	0.01	0.03	0.02	0.02	0.02	0.03	0.00
Ca	0.00	0.00	0.00	0.00	0.00	0.00	0.00	0.00	0.00	0.00	0.00	0.00	0.00
Sum in C	5.00	5.00	5.00	5.00	5.00	5.00	5.00	5.00	5.00	5.00	5.00	5.00	5.00
Fe ²⁺	1.80	0.00	0.00	0.00	0.04	0.00	0.00	0.00	0.00	0.00	0.07	0.00	1.51
Mn	0.09	0.00	0.00	0.00	0.02	0.00	0.00	0.00	0.00	0.00	0.01	0.00	0.10
Ca	0.11	1.87	1.79	1.86	1.94	1.81	0.03	1.84	1.72	1.71	1.76	1.97	0.40
Na	0.00	0.13	0.21	0.14	0.00	0.19	0.03	0.16	0.28	0.29	0.16	0.03	0.00
Sum in B	2.00	2.00	2.00	2.00	2.00	2.00	2.00	2.00	2.00	2.00	2.00	2.00	2.00
Ca	0.00	0.00	0.00	0.00	0.00	0.00	0.00	0.00	0.00	0.00	0.00	0.00	0.00
Na	0.06	0.52	0.49	0.34	0.17	0.35	0.07	0.30	0.46	0.45	0.36	0.07	0.04
K	0.06	0.06	0.05	0.04	0.01	0.03	0.01	0.02	0.03	0.03	0.02	0.01	0.00
Sum in A	0.11	0.58	0.54	0.39	0.19	0.38	0.07	0.32	0.49	0.49	0.38	0.08	0.04
Cl	0.00	0.37	0.13	0.17	0.02	0.08	0.01	0.06	0.01	0.00	0.04	0.00	0.00
Mg#	68.98	56.58	67.86	67.84	74.92	78.72		55.01	74.00	98.19	85.06	63.39	72.94

Table 2 (continued).

Sample number:	118-735B-25R-1 (Piece 3, 12–17 cm)		118-735B-26R-2 (Piece 2A, 8–12 cm)		118-735B-36R-1 (Piece 3, 17–20 cm)		118-735B-37R-2 (Piece 1H, 113–117 cm)							
	Mg-hb avg of 6 w/An ₄₆	Act-hb	Mg-hb avg of 2	Act avg of 2	Mg-hb avg of 5	Cumm	Mg-hst-hb avg of 3	Ed-hb avg of 2	Mg-hb avg of 2	Act-hb	Act-hb	Act	Act avg of 2	Mg-cumm
SiO ₂	44.17	50.89	47.29	52.73	46.05	56.06	44.32	44.51	46.16	50.57	48.04	51.18	54.82	56.78
TiO ₂	1.48	0.38	0.34	0.00	1.34	0.00	1.09	0.57	0.63	0.45	0.58	0.26	0.11	0.00
Al ₂ O ₃	9.94	3.90	8.85	1.29	7.67	0.16	11.04	9.42	8.43	3.05	4.36	2.68	1.09	0.85
FeO*	14.75	12.68	11.82	19.58	16.71	20.20	12.21	16.80	16.46	19.33	21.75	20.80	13.24	14.20
MnO	0.17	0.14	0.12	0.46	0.23	0.73	0.20	0.16	0.22	0.26	0.31	0.39	0.24	0.79
MgO	12.40	15.87	15.23	11.02	12.43	20.91	14.25	11.58	11.87	11.32	9.86	11.31	17.07	24.68
CaO	11.37	11.99	11.44	12.53	11.63	0.76	11.31	11.62	11.33	11.43	10.78	9.85	10.59	0.75
Na ₂ O	2.01	0.85	1.98	0.05	1.87	0.05	2.46	2.14	1.91	0.81	1.21	1.07	0.26	0.24
K ₂ O	0.49	0.05	0.15	0.01	0.40	0.01	0.29	0.38	0.15	0.18	0.27	0.11	0.02	0.01
Cl	0.36	0.03	0.25	0.00	0.19	0.00	0.00	0.44	0.51	0.28	0.51	0.29	0.03	0.01
Total	97.13	96.78	97.45	97.64	98.52	98.88	97.17	97.61	97.64	97.68	97.67	97.94	97.44	98.31
O = Cl	0.08	0.01	0.06	0.00	0.04	0.00	0.00	0.10	0.12	0.06	0.12	0.07	0.01	0.00
Total	97.04	96.77	97.40	97.64	98.48	98.88	97.17	97.51	97.53	97.62	97.55	97.87	97.43	98.31
Routine	13ECNK	13ECNK	13ECNK	13ECNK	13ECNK	15ENK	13ECNK	13ECNK	13ECNK	13ECNK	15ENK	15EK	15EK	15ENK
Si	6.53	7.34	6.78	7.84	6.74	7.95	6.42	6.61	6.80	7.49	7.33	7.55	7.85	7.89
Al	1.47	0.66	1.22	0.16	1.26	0.05	1.58	1.39	1.20	0.51	0.67	0.46	0.15	0.11
Sum in T	8.00	8.00	8.00	8.00	8.00	8.00	8.00	8.00	8.00	8.00	8.00	8.00	8.00	8.00
Al	0.26	0.00	0.28	0.07	0.07	-0.02	0.30	0.26	0.27	0.02	0.11	0.01	0.03	0.03
Fe ³⁺	0.62	0.63	0.78	0.09	0.64	0.05	0.79	0.61	0.64	0.49	0.01	0.67	0.16	0.01
Ti	0.17	0.04	0.04	0.00	0.15	0.00	0.12	0.06	0.07	0.05	0.07	0.03	0.01	0.00
Mg	2.73	3.41	3.25	2.44	2.71	4.42	3.08	2.56	2.61	2.50	2.24	2.49	3.64	5.11
Fe ²⁺	1.21	0.90	0.64	2.34	1.41	0.55	0.69	1.48	1.39	1.90	2.56	1.80	1.15	-0.15
Mn	0.02	0.02	0.02	0.06	0.03	0.00	0.02	0.02	0.03	0.03	0.00	0.00	0.00	0.00
Ca	0.00	0.00	0.00	0.00	0.00	0.00	0.00	0.00	0.00	0.00	0.00	0.00	0.00	0.00
Sum in C	5.00	5.00	5.00	5.00	5.00	5.00	5.00	5.00	5.00	5.00	5.00	5.00	5.00	5.00
Fe ²⁺	0.00	0.00	0.00	0.00	0.00	1.80	0.00	0.00	0.00	0.00	0.20	0.09	0.28	1.80
Mn	0.00	0.00	0.00	0.00	0.00	0.09	0.00	0.00	0.00	0.00	0.04	0.05	0.03	0.09
Ca	1.80	1.85	1.76	1.99	1.82	0.12	1.75	1.85	1.79	1.81	1.76	1.56	1.62	0.11
Na	0.20	0.15	0.24	0.01	0.18	0.00	0.25	0.15	0.21	0.19	0.00	0.31	0.07	0.00
Sum in B	2.00	2.00	2.00	2.00	2.00	2.00	2.00	2.00	2.00	2.00	2.00	2.00	2.00	2.00
Ca	0.00	0.00	0.00	0.00	0.00	0.00	0.00	0.00	0.00	0.00	0.00	0.00	0.00	0.00
Na	0.38	0.09	0.31	0.01	0.36	0.01	0.45	0.46	0.33	0.05	0.36	0.00	0.00	0.07
K	0.09	0.01	0.03	0.00	0.08	0.00	0.05	0.07	0.03	0.03	0.05	0.02	0.00	0.00
Sum in A	0.47	0.10	0.34	0.01	0.43	0.02	0.50	0.54	0.36	0.08	0.41	0.02	0.00	0.07
Cl	0.09	0.01	0.06	0.00	0.05	0.00	0.00	0.11	0.13	0.07	0.13	0.07	0.01	0.00
Mg#	69.26	79.05	83.53	51.01	65.85	65.35	81.72	63.53	65.52	56.76	44.80	56.76	71.86	75.70

Table 2 (continued).

Sample number:	118-735B-45R-4 (Piece 7, 136–140 cm)				118-735B-53R-4 (Piece 1B, 5–15 cm)		118-735B-54R-2 (Piece 1C, 32–34 cm)				118-735B-57R-2 (Piece 1B, 11–18 cm)		
	Mg-hast enc trem	Eden-hb	Mg-hb nxt cl-ap	Trem on cpx	Mg-hb	Cumm	Fe-hb	Fe-act-hb avg of 3	Fe-act-hb avg of 2	Cumm	Mg-hb	Mg-hb avg of 5	Act
SiO ₂	43.62	43.66	47.70	57.32	43.53	52.74	43.91	43.38	47.44	50.73	45.83	48.44	53.77
TiO ₂	1.97	2.00	1.29	0.05	2.20	0.00	1.00	0.75	0.42	0.00	0.30	1.33	0.22
Al ₂ O ₃	12.34	8.74	6.05	0.26	9.16	0.20	6.33	4.13	3.22	0.09	7.52	5.50	1.27
FeO*	8.36	18.62	17.08	3.82	18.88	26.62	30.24	23.20	30.35	30.67	18.90	15.81	13.67
MnO	0.13	0.15	0.20	0.63	0.30	1.05	0.41	0.39	0.57	0.78	0.09	0.32	0.19
MgO	16.13	10.29	12.51	23.22	9.62	14.45	3.57	9.16	6.29	12.84	10.59	12.99	15.42
CaO	12.27	11.33	11.51	12.64	10.11	1.10	10.43	10.28	7.21	0.48	12.01	10.49	11.88
Na ₂ O	2.93	2.39	1.85	0.12	2.29	0.09	1.14	0.84	0.62	0.06	1.29	1.72	0.40
K ₂ O	0.35	0.43	0.13	0.01	0.25	0.01	0.64	0.31	0.24	0.00	0.07	0.23	0.06
Cl	0.00	0.45	0.14	0.00	0.00	0.02	0.21	0.02	0.07	0.01	0.05	0.01	0.05
Total	98.10	98.06	98.46	98.07	96.34	96.28	97.88	97.47	96.41	95.66	96.65	96.86	96.93
O = Cl	0.00	0.10	0.03	0.00	0.00	0.00	0.05	0.00	0.02	0.00	0.01	0.00	0.01
Total	98.10	97.96	98.43	98.07	96.34	96.28	97.83	97.46	96.39	95.66	96.64	96.86	96.92
Routine	13ECNK	13ECNK	13ECNK	Fe ²⁺	13ECNK	15EK	13ECNK	15ENK	15EK	15ENK	13ECNK	13ECNK	15EK
Si	6.25	6.56	6.98	7.89	6.55	7.99	6.87	7.40	7.44	7.86	6.88	7.09	7.79
Al	1.76	1.44	1.03	0.11	1.45	0.01	1.13	0.60	0.56	0.14	1.12	0.91	0.21
Sum in T	8.00	8.00	8.00	8.00	8.00	8.00	8.00	8.00	8.00	8.00	8.00	8.00	8.00
Al	0.33	0.11	0.02	-0.07	0.18	0.03	0.04	0.12	0.03	-0.12	0.21	0.04	0.01
Fe ³⁺	0.36	0.45	0.57	0.00	0.79	0.01	0.89	-0.01	0.58	0.24	0.59	0.75	0.25
Ti	0.21	0.23	0.14	0.01	0.25	0.00	0.12	0.09	0.05	0.00	0.03	0.15	0.02
Mg	3.44	2.31	2.73	4.76	2.16	3.26	0.83	2.22	1.47	2.97	2.37	2.83	3.33
Fe ²⁺	0.64	1.89	1.52	0.31	1.58	1.70	3.07	2.58	2.88	1.91	1.79	1.19	1.38
Mn	0.02	0.02	0.03	0.00	0.04	0.00	0.05	0.00	0.00	0.00	0.01	0.04	0.00
Ca	0.00	0.00	0.00	0.00	0.00	0.00	0.00	0.00	0.00	0.00	0.00	0.00	0.00
Sum in C	5.00	5.00	5.00	5.00	5.00	5.00	5.00	5.00	5.00	5.00	5.00	5.00	5.00
Fe ²⁺	0.00	0.00	0.00	0.13	0.00	1.66	0.00	0.26	0.53	1.82	0.00	0.00	0.02
Mn	0.00	0.00	0.00	0.07	0.00	0.14	0.00	0.05	0.08	0.10	0.00	0.00	0.02
Ca	1.88	1.82	1.80	1.79	1.63	0.18	1.75	1.69	1.21	0.08	1.93	1.65	1.85
Na	0.12	0.18	0.20	0.00	0.37	0.03	0.25	0.00	0.19	0.00	0.07	0.35	0.11
Sum in B	2.00	2.00	2.00	2.00	2.00	2.00	2.00	2.00	2.00	2.00	2.00	2.00	2.00
Ca	0.00	0.00	0.00	0.07	0.00	0.00	0.00	0.00	0.00	0.00	0.00	0.00	0.00
Na	0.70	0.52	0.33	0.03	0.30	0.00	0.09	0.25	0.00	0.02	0.31	0.14	0.00
K	0.06	0.08	0.02	0.00	0.05	0.00	0.13	0.06	0.05	0.00	0.01	0.04	0.01
Sum in A	0.76	0.60	0.35	0.11	0.35	0.00	0.22	0.31	0.05	0.02	0.32	0.18	0.01
Cl	0.00	0.12	0.04	0.00	0.00	0.01	0.06	0.00	0.02	0.00	0.01	0.00	0.01
Mg#	84.28	54.93	64.19	91.54	57.70	49.24	21.31	43.87	30.17	44.27	57.02	70.50	70.34

Table 2 (continued).

Sample number:	118-735B-58R-1 (Piece 10, 47-51 cm)				118-735B-58R-2 (Piece 1B, 10-17 cm)			118-735B-65R-2 (Piece 1B, 18-25 cm)			118-735B-68R-3 (Piece 5, 62-64 cm)		
	Tsch-hb	Mg-hb	Act-hb	Trem avg of 2	Mg-hb	Act-hb	Trem	Ed-hb	Mg-hb	Act	Mg-hast	Act-hb avg of 2	Trem avg of 2
SiO ₂	43.64	46.89	50.61	56.47	47.74	51.54	57.75	44.57	49.39	55.91	42.38	51.92	58.03
TiO ₂	1.69	0.62	0.42	0.11	0.88	0.42	0.04	1.43	1.22	0.08	0.03	0.08	0.06
Al ₂ O ₃	10.58	8.52	5.32	0.86	8.02	4.23	0.77	10.09	6.97	1.83	15.30	5.76	0.73
FeO*	13.68	11.25	10.75	5.39	11.58	13.32	4.70	13.84	7.51	5.51	11.95	7.01	3.70
MnO	0.12	0.23	0.09	0.09	0.20	0.13	0.14	0.16	0.08	0.16	0.12	0.11	0.09
MgO	12.89	16.29	16.34	22.10	15.56	15.29	22.66	13.13	18.13	21.57	13.30	18.87	22.75
CaO	11.48	10.81	12.28	12.05	11.34	11.89	11.99	11.41	11.60	12.02	11.66	12.36	12.73
Na ₂ O	1.99	2.12	1.11	0.22	1.85	0.87	0.25	2.40	1.49	0.48	2.85	1.18	0.26
K ₂ O	0.46	0.25	0.05	0.00	0.27	0.04	0.00	0.23	0.11	0.00	0.18	0.09	0.01
Cl	0.05	0.00	0.03	0.01	0.00	0.05	0.00	0.07	0.00	0.00	0.17	0.05	0.01
Total	96.58	96.98	97.00	97.28	97.44	97.78	98.30	97.33	96.50	97.56	97.94	97.41	98.35
O = Cl	0.01	0.00	0.01	0.00	0.00	0.01	0.00	0.02	0.00	0.000	0.04	0.01	0.00
Total	96.57	96.98	96.99	97.28	97.44	97.77	98.30	97.31	96.50	97.56	97.90	97.40	98.35
Routine	13ECNK	13ECNK	13ECNK	15ENK	13ECNK	13ECNK	15EK	13ECNK	13ECNK	15ENK	13ECNK	13ECNK	15ENK
Si	6.44	6.68	7.26	7.84	6.83	7.37	7.89	6.52	6.99	7.77	6.10	7.27	7.93
Al	1.56	1.32	0.74	0.16	1.17	0.63	0.11	1.48	1.01	0.23	1.90	0.73	0.07
Sum in T	8.00	8.00	8.00	8.00	8.00	8.00	8.00	8.00	8.00	8.00	8.00	8.00	8.00
Al	0.28	0.11	0.16	-0.02	0.18	0.09	0.01	0.27	0.15	0.07	0.69	0.22	0.04
Fe ³⁺	0.63	1.15	0.40	0.09	0.77	0.56	0.16	0.60	0.66	0.01	0.78	0.45	0.00
Ti	0.19	0.07	0.05	0.01	0.10	0.05	0.00	0.16	0.13	0.01	0.00	0.01	0.01
Mg	2.83	3.46	3.49	4.58	3.32	3.26	4.61	2.86	3.82	4.47	2.85	3.94	4.63
Fe ²⁺	1.06	0.19	0.89	0.34	0.62	1.04	0.21	1.10	0.23	0.44	0.66	0.37	0.32
Mn	0.02	0.03	0.01	0.00	0.02	0.02	0.00	0.02	0.01	0.00	0.02	0.01	0.00
Ca	0.00	0.00	0.00	0.00	0.00	0.00	0.00	0.00	0.00	0.00	0.00	0.00	0.00
Sum in C	5.00	5.00	5.00	5.00	5.00	5.00	5.00	5.00	5.00	5.00	5.00	5.00	5.00
Fe ²⁺	0.00	0.00	0.00	0.20	0.00	0.00	0.16	0.00	0.00	0.19	0.00	0.00	0.10
Mn	0.00	0.00	0.00	0.01	0.00	0.00	0.02	0.00	0.00	0.02	0.00	0.00	0.01
Ca	1.81	1.65	1.89	1.79	1.74	1.82	1.75	1.79	1.76	1.79	1.80	1.85	1.86
Na	0.19	0.35	0.11	0.00	0.26	0.18	0.07	0.21	0.24	0.00	0.20	0.15	0.03
Sum in B	2.00	2.00	2.00	2.00	2.00	2.00	2.00	2.00	2.00	2.00	2.00	2.00	2.00
Ca	0.00	0.00	0.00	0.00	0.00	0.00	0.00	0.00	0.00	0.00	0.00	0.00	0.00
Na	0.38	0.24	0.20	0.06	0.25	0.06	0.00	0.47	0.17	0.13	0.59	0.17	0.04
K	0.09	0.05	0.01	0.00	0.05	0.01	0.00	0.04	0.02	0.00	0.03	0.02	0.00
Sum in A	0.47	0.28	0.21	0.06	0.30	0.07	0.00	0.51	0.19	0.13	0.63	0.19	0.05
Cl	0.01	0.00	0.01	0.00	0.00	0.01	0.00	0.02	0.00	0.00	0.04	0.01	0.00
Mg#	72.77	94.82	79.62	89.61	84.27	75.88	92.46	72.27	94.32	87.61	81.27	91.85	91.62

Table 2 (continued).

Sample number:	118-735B-73R-6 (Piece 6C, 60–65 cm)			118-735B-78R-4 (Piece 5B, 54–59 cm)			118-735B-81R-2 (Piece 1C, 23–31 cm)			118-735B-85R-4 (Piece 1C, 17–25 cm)		118-735B-87R-7 (Piece 1C, 15–17 cm)
	Tsch-hb	Mg-hb	Act-hb	Tsch-hb w/An ₆₆	Act w/An ₁₇	Cumm avg of 4	Act w/An ₃₀	Fe-act w/zircon	Cumm avg of 2	Fe-prg-hb	Act	Edenite
SiO ₂	43.49	46.39	50.04	44.55	54.34	53.72	51.45	52.06	51.68	43.27	54.74	47.60
TiO ₂	0.02	0.27	0.29	1.45	0.00	0.00	0.22	0.04	0.14	3.28	0.15	1.07
Al ₂ O ₃	11.72	8.24	4.14	10.91	0.55	0.20	2.37	1.01	0.50	11.51	1.58	7.32
FeO*	15.46	17.89	18.67	11.36	16.30	26.31	17.92	21.89	27.76	13.17	10.00	11.89
MnO	0.10	0.12	0.22	0.18	0.43	1.04	0.54	0.36	0.84	0.24	0.19	0.12
MgO	12.04	10.38	10.70	14.15	15.48	15.64	15.09	10.31	13.97	12.11	18.29	15.18
CaO	11.45	11.34	12.05	11.56	9.98	0.78	8.11	11.64	1.52	10.80	12.11	11.68
Na ₂ O	2.01	1.06	0.54	2.18	0.11	0.06	0.47	0.21	0.11	2.88	0.40	2.19
K ₂ O	0.09	0.06	0.05	0.38	0.05	0.01	0.04	0.01	0.01	0.30	0.03	0.09
Cl	0.04	0.01	0.00	0.00	0.02	0.01	0.04	0.00	0.00	0.00	0.00	0.05
Total	96.42	95.76	96.70	96.72	97.26	97.75	96.25	97.53	96.51	97.56	97.49	97.19
O = Cl	0.01	0.00	0.00	0.00	0.00	0.00	0.01	0.00	0.00	0.00	0.00	0.01
Total	96.41	95.76	96.70	96.72	97.26	97.75	96.24	97.53	96.51	97.56	97.49	97.18
Routine	13ECNK	13ECNK	13ECNK	13ECNK	15ENK	15ENK	15ENK	15ENK	15ENK	13ECNK	15ENK	13ECNK
Si	6.40	6.94	7.49	6.49	7.93	7.98	7.64	7.83	7.85	6.35	7.79	6.90
Al	1.60	1.06	0.51	1.51	0.07	0.02	0.36	0.17	0.15	1.65	0.22	1.10
Sum in T	8.00	8.00	8.00	8.00	8.00	8.00	8.00	8.00	8.00	8.00	8.00	8.00
Al	0.44	0.40	0.22	0.36	0.03	0.02	0.05	0.01	-0.06	0.34	0.05	0.15
Fe ³⁺	0.95	0.64	0.20	0.54	0.00	-0.01	0.12	0.09	0.15	0.31	0.02	0.46
Ti	0.00	0.03	0.03	0.16	0.00	0.00	0.03	0.01	0.02	0.36	0.02	0.12
Mg	2.64	2.32	2.39	3.07	3.37	3.46	3.34	2.31	3.16	2.65	3.88	3.28
Fe ²⁺	0.96	1.60	2.14	0.85	1.61	1.54	1.47	2.59	1.74	1.31	1.04	0.98
Mn	0.01	0.02	0.03	0.02	0.00	0.00	0.00	0.00	0.00	0.03	0.00	0.02
Ca	0.00	0.00	0.00	0.00	0.00	0.00	0.00	0.00	0.00	0.00	0.00	0.00
Sum in C	5.00	5.00	5.00	5.00	5.00	5.00	5.00	5.00	5.00	5.00	5.00	5.00
Fe ²⁺	0.00	0.00	0.00	0.00	0.39	1.74	0.64	0.08	1.65	0.00	0.13	0.00
Mn	0.00	0.00	0.00	0.00	0.05	0.13	0.07	0.05	0.11	0.00	0.02	0.00
Ca	1.81	1.82	1.93	1.80	1.56	0.12	1.29	1.88	0.25	1.70	1.85	1.81
Na	0.19	0.18	0.07	0.20	0.00	0.00	0.00	0.00	0.00	0.30	0.00	0.19
Sum in B	2.00	2.00	2.00	2.00	2.00	2.00	2.00	2.00	2.00	2.00	2.00	2.00
Ca	0.00	0.00	0.00	0.00	0.00	0.00	0.00	0.00	0.00	0.00	0.00	0.00
Na	0.38	0.13	0.09	0.42	0.03	0.02	0.14	0.06	0.03	0.52	0.11	0.43
K	0.02	0.01	0.01	0.07	0.01	0.00	0.01	0.00	0.00	0.06	0.01	0.02
Sum in A	0.40	0.14	0.10	0.49	0.04	0.02	0.14	0.06	0.03	0.57	0.12	0.45
Cl	0.01	0.00	0.00	0.00	0.01	0.00	0.01	0.00	0.00	0.00	0.00	0.01
Mg#	73.45	59.13	52.76	78.35	62.85	51.34	61.29	46.44	48.34	66.98	76.78	76.97

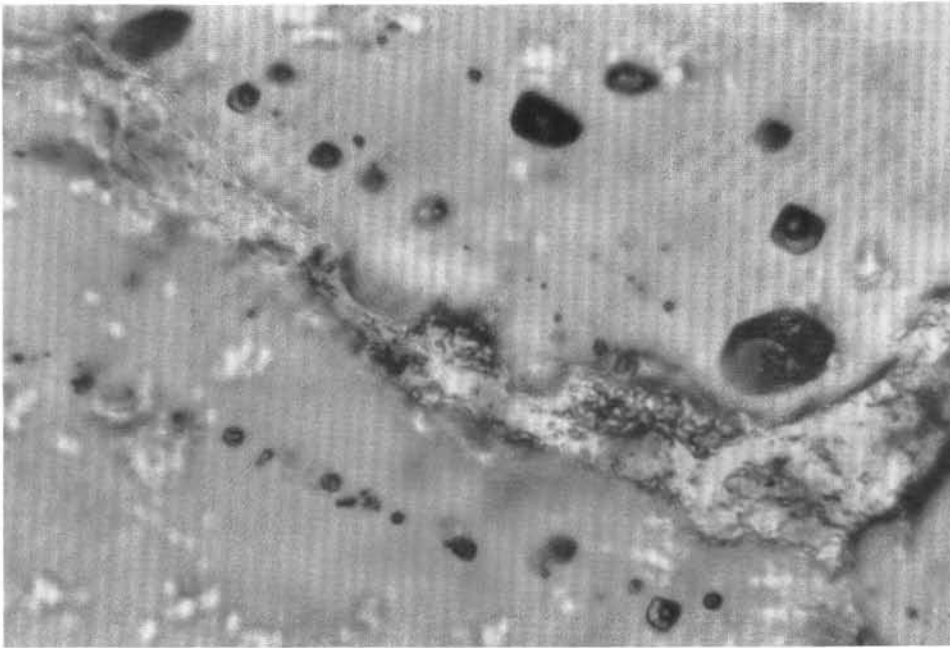


Figure 10. Close-up photomicrograph of fluid inclusions in quartz from the trondhjemite, Sample 118-735B-54R-2 (Piece 1C, 32–34 cm). Field of view is 0.16 mm wide. Inclusions are both solitary and aligned along healed fracture surfaces in the quartz.

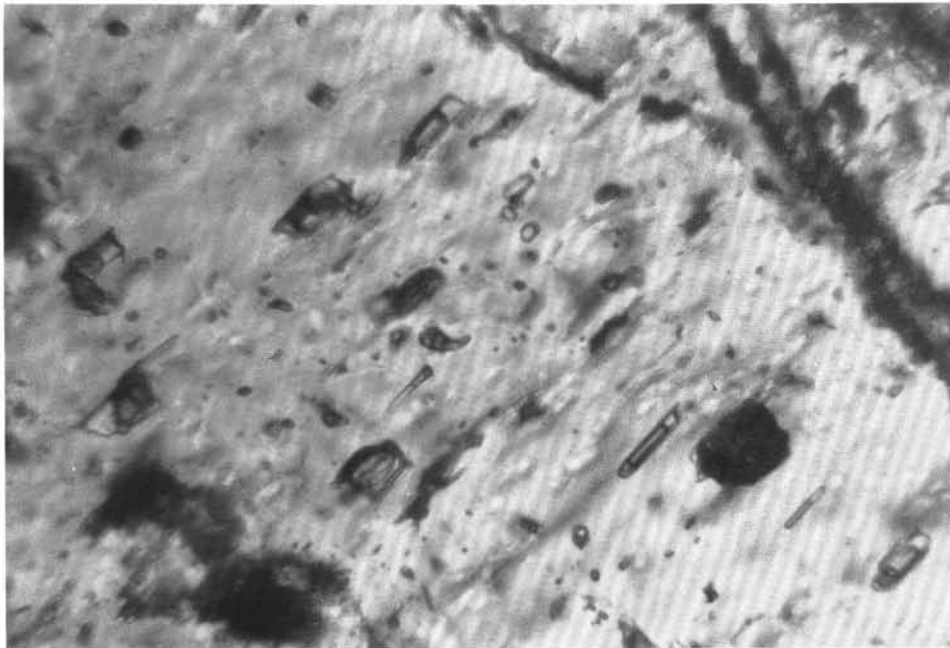


Figure 11. Photomicrograph showing fluid inclusions in vein diopside, Sample 118-735B-70R-1 (Piece 2B, 39–49 cm). Field of view is 0.2 mm wide. Note that most inclusions are rectangular or tubular, aligned parallel to the host diopside's c-axis (i.e., parallel to the intersection of cleavage).

rithm that assigns iron to these two oxidation states based on certain crystallochemical assumptions (see Robinson et al., 1982, for details). Examples of two recalculations are shown in Table 3. The choice of which recalculation scheme to use can be arbitrary. For many amphiboles, only one scheme provides a reasonable formula, but for others, several recal-

culations are allowed. In general, hornblendes are best recalculated using the "13ECNK" procedure, which fills the tetrahedral cation site with 8 atoms, the C site with 5 atoms, and excludes calcium, sodium, and potassium from the C site (forcing them into B and A; thus, the recalculation is based on 13 atoms, except C_0N_0K , Na, and K). For many of

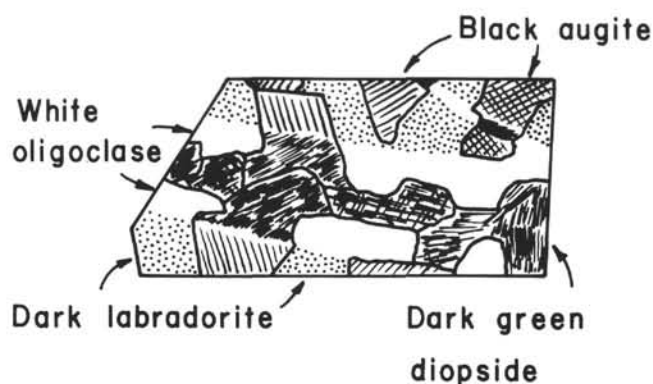


Figure 12. Sketch of a small sawn chip from Sample 118-735B-70R-1 (Piece 2B, 39–49 cm) showing an 8-mm wide leucocratic diopside-bearing vein cutting a fresh gabbro. Note that the diopside seems to have grown epitaxially on the augite of the host gabbro. Note also the small apophysis in the upper right.

the more aluminous amphiboles from Hole 735B, both the 13ECNK and 15EK schemes produce good formulas. The former has more ferric iron than the latter, and the classification of the amphibole then is either a pargasitic variety (using 15EK, with low ferric iron), or a hastingsitic variety (using 13ECNK, with more ferric iron). The distinction is not important, but because many amphiboles require the 13ECNK procedure to produce a legitimate formula, we have chosen to use 13ECNK as much as possible to be consistent.

The main variable that helps to differentiate these amphiboles is the aluminum content (Fig. 13). High-aluminum varieties are tschermakitic hornblendes, and pargasitic hornblendes or magnesio-hastingsitic hornblendes. The more abundant, intermediate-aluminum amphiboles are magnesio-hornblendes, with fewer ferro-hornblendes. Lower-aluminum varieties are actinolitic hornblendes. Low-aluminum actinolites and ferro-actinolites are common in some samples. A general trend shown in Figure 13 is that the more aluminous varieties are also apt to contain more alkali elements (Na, K); thus, there are more hastingsitic/pargasitic examples than tschermakitic ones.

Sometimes, high-aluminum hornblendes can be linked with an earlier petrographic mode that is interpreted as a high-temperature metamorphic or even late magmatic amphibole. For example, the magnesio-hastingsite in Sample 118-735B-2D-2 (Piece 6, 36–39 cm), a veined mylonitic metagabbro, occurs as small brown grains within clinopyroxene porphyroclasts and in the tails of those porphyroclasts. The hornblende in the veinlets cutting this sample, which is a green variety, is magnesio-hornblende with lower aluminum. Another example is Sample 118-735B-1D-1 (Piece 1, 0–5 cm), a foliated metagabbro. An aluminous hornblende (with 11 wt% Al_2O_3) occurs with a calcic plagioclase (andesine An_{46}), and a later generation less aluminous magnesio-hornblende (5 wt% Al_2O_3) occurs adjacent to a more sodic plagioclase (oligoclase An_{20}). In many other cases the high- and lower-aluminum hornblendes form a continuum of compositions, as in Sample 118-735B-7D-1 (Piece 2A, 10–16 cm), a foliated metagabbro (Fig. 14).

Many of the metagabbros contain hornblende both as a replacement of clinopyroxene, often forming a foliation, and as veinlets cross-cutting the foliation at a high angle. There is often no significant chemical difference between these two

hornblende types (e.g., Samples 118-735B-12R-1 [Piece 5D, 65–68 cm] and 118-735B-14R-3 [Piece 2A, 31–35 cm]).

Amphiboles are generally homogeneous, except where they are being replaced (e.g., actinolite replacing magnesio-hornblende). Some of the late-stage actinolitic amphiboles, notably in those samples having abundant green hornblende veins, exhibit dramatic oscillatory zonation near voids ormiarolitic cavities (Fig. 4). This indicates that during vein filling, oscillatory fluctuations in fluid parameters (such as temperature, pressure, and individual component activities) must have occurred.

A particularly wide range of amphibole composition occurs in Sample 118-735B-37R-2 (Piece 1H, 113–117 cm), which is from a brecciated zone at the Unit II/III contact. A continuum exists from high-aluminum tschermakitic and hastingsitic/pargasitic hornblendes through low-aluminum actinolite. Plagioclases in this sample also exhibit a remarkably wide range of composition from labradorite through oligoclase (see Table 1 and feldspar composition section below).

Notably iron-rich amphiboles occur in Sample 118-735B-54R-2 (Piece 1C, 32–34 cm), a trondhjemite within Unit IV. Amphiboles are classified as ferro-hornblende and ferro-actinolitic hornblende.

In addition to calcic amphiboles, iron-magnesium amphiboles occur in some gabbros (Stakes et al., this volume), but not within the veins. Most appear to be clin amphiboles, and analyses (Table 3) indicate that most are cummingtonite, with minor magnesio-cummingtonite in some samples. These amphiboles occur within reaction coronas on mafic igneous minerals, usually orthopyroxene, but also clinopyroxene and olivine. Coronas typically also contain one or more of the following: tremolite, mica, actinolite, and chlorite.

Chlorine is a significant halogen in many Hole 735B hornblendes and may be used to infer qualitatively the nature of the fluid present during hornblende growth (e.g., Ito and Anderson, 1983; Vanko, 1986). Chlorine is most abundant in the aluminous magnesio-hornblendes that occur as veinlets and within foliation, particularly within the upper Units I, II, and III. Chlorine is low in early high-temperature aluminous hornblende (e.g., the brown magnesio-hastingsite associated with pyroxene porphyroclasts in Sample 118-735B-2D-2 [Piece 6, 36–39 cm]). It is also low in actinolitic hornblendes and actinolite.

Magnesio-hornblende in samples from Units I, II, and III commonly contains a few tenths of a percent of chlorine, with some values as high as 1.5 wt%. These levels of chlorine are the same as those seen in many other oceanic metagabbro suites that have been shown to result from seawater interaction (e.g., Ito and Anderson, 1983; Batiza and Vanko, 1985; Vanko, 1986; Mevel, 1988). Magnesio-hornblendes in samples from Units IV, V, and VI contain noticeably less chlorine, perhaps indicating that the fluids attending amphibole growth deep in the hole were less saline. Exceptions to this were noted in Sample 118-735B-68R-3 (Piece 5, 62–64 cm), a veined metagabbro from Unit V, and Sample 118-735B-54R-2 (Piece 1C, 32–34 cm), the trondhjemite located within Unit IV.

Feldspars

All of the feldspars in Hole 735B are plagioclase feldspars. The maximum orthoclase content is normally less than 2 mol%, but one sample contains up to 7 mol% orthoclase component in albite. Representative analyses are shown in Table 4.

Some samples contain essentially a single feldspar type: Sample 118-735B-2D-2 (Piece 6, 36–39 cm), the mylonitic gabbro with a cross-cutting hornblende-plagioclase vein, con-

Table 3. Examples of amphibole analysis recalculations, Hole 735B samples.

	Magnesio-hornblende				Ferro-pargasitic hornblende			
SiO ₂	45.18				42.23			
TiO ₂	0.38				0.21			
Al ₂ O ₃	8.49				12.15			
FeO*	17.4				14.44			
MnO	0.24				0.21			
MgO	12.27				11.99			
CaO	11.27				11.55			
Na ₂ O	2.17				2.97			
K ₂ O	0.2				0.31			
Cl	0.96				0.01			
Total	98.56				96.07			
O = Cl	0.22				0			
Total	98.34				96.07			
	Fe ²⁺	15ENK	15EK	13ECNK	Fe ²⁺	15ENK	15EK	13ECNK
Si	6.779	6.737	6.466	6.635	6.397	6.384	6.034	6.322
Al	1.221	1.263	1.534	1.365	1.603	1.616	1.966	1.678
Sum in T	8	8	8	8	8	8	8	8
Al	0.281	0.23	-0.1	0.106	0.568	0.551	0.082	0.467
Fe ³⁺	-0.002	0.283	2.118	0.973	-0.003	0.086	2.605	0.538
Ti	0.043	0.043	0.041	0.042	0.024	0.024	0.023	0.024
Mg	2.744	2.727	2.617	2.685	2.707	2.701	2.553	2.675
Fe ²⁺	1.934	1.718	-0.035	1.164	1.705	1.637	-0.88	1.27
Mn	0	0	0.029	0.03	0	0	0.025	0.027
Ca	0	0	0.331	0	0	0	0.591	0
Sum in C	5	5	5	5	5	5	5	5
Fe ²⁺	0.251	0.169	0	0	0.128	0.102	0	0
Mn	0.031	0.03	0	0	0.027	0.027	0	0
Ca	1.718	1.801	1.398	1.773	1.845	1.871	1.177	1.853
Na	0	0	0.602	0.227	0	0	0.823	0.147
Sum in B	2	2	2	2	2	2	2	2
Ca	0.093	0	0	0	0.029	0	0	0
Na	0.631	0.627	0	0.391	0.872	0.871	0	0.715
K	0.038	0.038	0.037	0.037	0.06	0.06	0.057	0.059
Sum in A	0.763	0.665	0.037	0.429	0.962	0.93	0.057	0.774
Cl	0.244	0.243	0.233	0.239	0.003	0.003	0.002	0.003

Explanation: Two electron microprobe analyses were recalculated based on various crystallo-chemical assumptions. The first is considered a magnesio-hornblende, according to the 13ECNK recalculation. Had the 15ENK been chosen, the mineral would be classified as an edenitic hornblende instead. We chose the 13ECNK procedure to be consistent, because many other analyses give poor formulas using the 15ENK procedure. In the second example, both the 15ENK and 13ECNK procedures result in a ferroan pargasitic hornblende. Note that the Fe²⁺ routine yields allowable formulas for both examples; however, it is unlikely that these minerals contain no ferric iron. Note also that the 15EK procedures yield poor formulas (all ferric iron, and fewer cations in the C site). See Robinson et al. (1982) for details about calculation procedures.

tains labradorite (An₅₅₋₅₀) both as an accessory in the vein and as neocrystalline mosaic in the gabbro. Several other mylonitic or metagabbros listed in Table 1 also have a uniform igneous or metamorphic plagioclase composition.

Many samples have complex plagioclase relationships. Veined gabbros commonly contain igneous plagioclase with metamorphic feldspar in veinlets cutting the original grains and forming along grain boundaries (Fig. 5, Table 4). Samples 118-735B-25R-1 (Piece 3, 12–17 cm) and 118-735B-26R-2 (Piece 2A, 8–12 cm), for example, have andesine veins within igneous labradorite. Samples 118-735B-63R-6 (Piece 5A, 94–98 cm) and 118-735B-70R-1 (Piece 2B, 39–49 cm) have oligoclase veins cutting igneous labradorite.

Three or more distinct plagioclase populations occur in a few samples. Sample 118-735B-35R-2 (Piece 4G, 102–106 cm) is a metagabbro containing a shear zone. Primary igneous plagioclase has been altered to andesine/oligoclase, and albite with up to 7 mol% orthoclase component occurs within the shear. Plagioclase from the major breccia zone at the Unit II/III contact (Sample 118-735B-37R-2 [Piece 1H, 113–117 cm]) is labradorite with successive generations of andesine and oligoclase. As noted

above, this sample also has a broad range of hornblende compositions from aluminum-rich to aluminum-poor. Metagabbro samples 118-735B-58R-1 (Piece 10, 47–51 cm), 118-735B-63R-6 (Piece 5a, 94–98 cm), 118-735B-70R-2 (Piece 2, 8–10 cm), and 118-735B-81R-2 (Piece 1C, 23–31 cm) are all other examples of metagabbros with igneous labradorite, metamorphic or hydrothermal andesine, and later hydrothermal oligoclase and/or albite. Notably, these gabbros occur within Units V and VI and are associated with late-stage centimeter-scale leucocratic veining.

Plagioclase in the trondhjemite sample (118-735B-54R-2 [Piece 1C, 32–34 cm]) ranges from andesine (An₃₂) through albite (An₅).

Compositions of Other Secondary Minerals

Table 5 contains some representative microprobe analyses of several other secondary minerals, and data also are summarized in Table 1. Chlorite is an accessory mineral in many metagabbros, where it forms as a minor replacement of plagioclase and mafic minerals. It is neither restricted to nor particularly abundant in any lithologic unit. Chlorite compo-

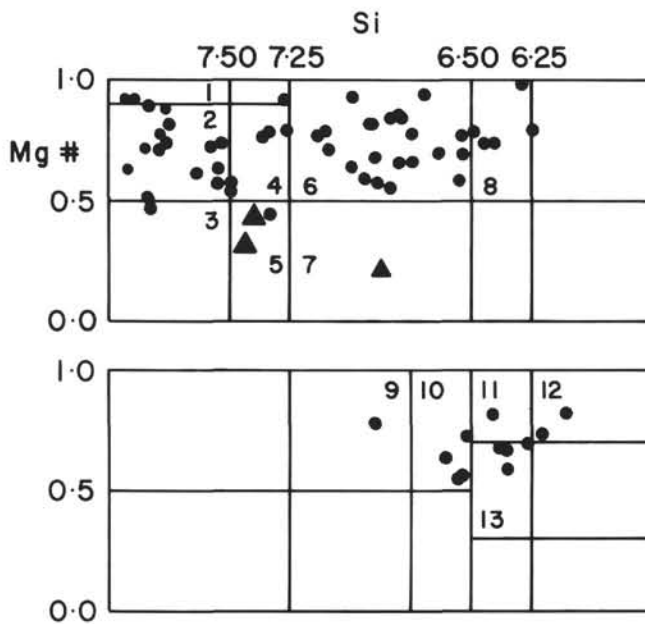


Figure 13. Plot of amphibole compositions listed in Table 2. This diagram, after Leake (1978), plots atomic Si vs. the atomic Mg number $[Mg/(Mg+Fe^{2+})]$. The upper rectangle is for those compositions with Na + K in the A site less than 0.50, and the lower rectangle is for those with Na + K in A greater than or equal to 0.50. The numbers within individual fields represent the following amphibole names: 1-tremolite, 2-actinolite, 3-ferro-actinolite, 4-actinolitic hornblende (hb), 5-ferro-actinolitic hb, 6-magnesio-hb, 7-ferro-hb, 8-tschermakitic hb, 9-edenite, 10-edenitic hb, 11-magnesio-hastingsitic or pargasitic hb, 12-magnesio-hastingsite or pargasite, 13-magnesian hastingsitic or ferroan pargasitic hb. The three triangle symbols represent ferroan amphiboles from the trondhjemite, Sample 118-735B-54R-2 (Piece 1C, 32–34 cm).

sitions range from magnesian to iron-rich, and most are classified as ripidolite (a ferroan clinocllore) using the Hey nomenclature (Deer et al., 1966). Pale magnesian chlorite was observed at the outermost rim of many of the more extensively developed coronitic replacements of mafic phases in metagabbros. In contrast, green iron-rich chlorite is abundant in many late-stage vein and breccia assemblages.

Diopside occurs as a replacing phase, but more commonly as a vein-filling phase in Units III, V, VI, and at the base of Unit II. This diopside has a paucity of nonquadrilateral components relative to igneous augite (Table 5), indicating a lower-temperature hydrothermal origin (subsolidus, but $\geq 300^{\circ}\text{C}$ [Bird et al., 1984; 1986]). In addition, many diopsides contain abundant fluid inclusions (see section below).

Epidote group minerals also occur in Units II through VI, with a greater abundance in the lower units (III, V, VI). They form as replacements of plagioclase and other igneous minerals and, more commonly, as bladed grains within veins and alteration zones. Compositions range from clinzoisite, or 0% pistacite component (Ps_0 , where Ps is 100 times atomic $Fe^{3+}/[Fe^{3+}+Al]$) up to Ps_{17} (Table 5). Epidotes that occur in altered or brecciated samples contain both low- and higher-iron compositions, and epidotes in diopside-bearing veins have low-iron compositions (Table 5).

Titanite is a common accessory phase in metagabbros and veins from Units III, V, and VI. Vein titanites typically have a rosey or pink tint, suggesting the presence of trace amounts of rare earth elements (Deer et al., 1966).

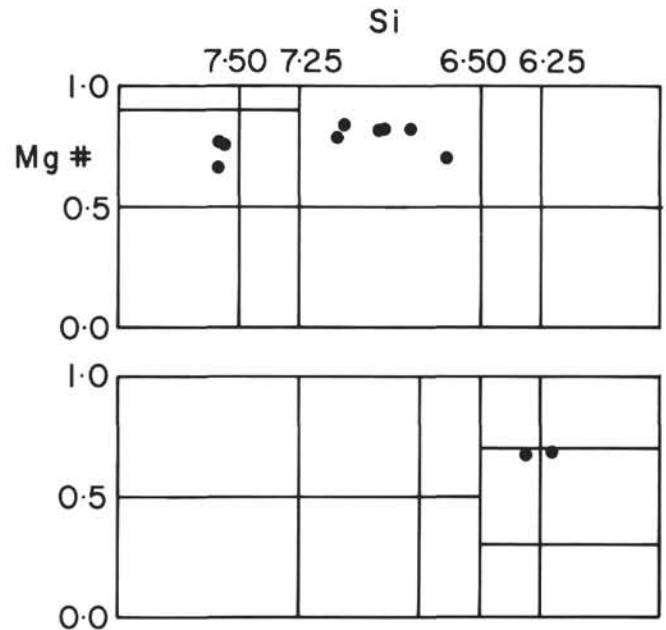


Figure 14. Plot of amphibole compositions from a single thin section of Sample 118-735B-7D-1 (Piece 2A, 10–16 cm), a foliated metagabbro. Fields are the same as in Figure 13. These analyses demonstrate the wide continuous range of compositions resulting from metamorphism that commenced in the amphibolite facies and continued into greenschist facies (see text for details).

Accessory mica occurs in some metagabbro and trondhjemite. In the gabbros, phlogopite is associated with alteration coronas on mafic phases. In the trondhjemite, biotite is an interstitial accessory mineral; it contains 0.2 to 0.3 wt% chlorine (Table 5), and a small fluorine peak was observed in the X-ray spectrum. One set of biotite analyses from a Unit VI metagabbro has up to 0.4 wt% chlorine. In contrast, a phlogopite from a metagabbro has essentially no chlorine (0.01 wt%, which is near the detection limit).

Calcite as late-stage veinlets measuring up to several millimeters across occurs throughout Hole 735B. Calcite has not been analyzed chemically, but X-ray diffraction confirms that the carbonate vein in Sample 118-735B-38R-4 (Piece 7B, 140–143 cm) is calcite. The strontium concentration and strontium isotopic ratio of vein calcite from this sample suggests crystallization from a low-temperature seawater-type fluid at around 10 ± 1 Ma ago (S. Hart, pers. comm., 1988). Other secondary accessory minerals noted are listed in Tables 1 and 5, and some analyses are presented in Table 1.

Fluid Inclusions

Fluid inclusions occur within some plagioclase, hornblende, diopside, apatite, and quartz. The fluids in these inclusions offer us an opportunity to infer the chemical and physical characteristics of the fluids that have played a role in the alteration of Hole 735B; the evidence demonstrates that multiple fluid types were present. Combined with mineral chemical and isotopic data, these fluid inclusions provide constraints on estimates of temperature and pressure of the fluid phase during hydrothermal alteration.

Igneous plagioclase in the samples that we have studied, all of which occur in or near altered zones, typically contains widely spaced trails of tiny (several micrometers) inclusions. These appear to contain either a dense fluid with one or more tiny, usually birefringent daughter crystals, or a low-density

Table 4. Representative feldspar analyses.

Sample number:	118-735B-2D-2 (Piece 6, 36–39 cm)		118-735B-22R-3 (Piece 5A, 112–115 cm)		118-735B-25R-1 (Piece 3, 12–17 cm)			118-735B-26R-2 (Piece 2A, 8–12 cm)		118-735B-54R-2 (Piece 1C, 32–34 cm)		
	Calcic igneous	Calcic igneous	Calcic igneous	Vein	Calcic igneous	Meta-morphic	Veinlets	Calcic igneous	Vein	Xeno-cryst	Adjacent to apatite	
SiO ₂	54.43	54.65	53.77	61.58	52.19	56.78	62.49	52.96	57.94	60.29	64.60	67.49
Al ₂ O ₃	29.27	28.79	30.03	25.08	31.04	27.56	24.64	30.41	27.36	25.19	22.24	20.91
Fe ₂ O ₃	0.23	0.09	0.08	0.01	0.07	0.33	0.35	0.31	0.10	0.20	0.24	0.12
MgO	0.02	0.01	0.01	0.01	0.00	0.00	0.00	0.00	0.03	0.00	0.00	0.00
CaO	11.02	10.40	11.96	6.02	13.28	9.03	5.15	12.54	8.80	6.20	3.06	0.94
Na ₂ O	4.98	5.47	4.64	7.71	3.94	6.08	8.26	4.20	6.22	7.34	9.00	10.27
K ₂ O	0.02	0.01	0.01	0.03	0.02	0.02	0.02	0.01	0.02	0.29	0.25	0.08
Total	99.95	99.43	100.50	100.42	100.53	99.79	100.90	100.43	100.47	99.52	99.40	99.81
Atoms based on 8 oxygens												
Si	2.45	2.47	2.42	2.72	2.35	2.55	2.74	2.39	2.58	2.69	2.86	2.95
Al	1.56	1.54	1.59	1.30	1.65	1.46	1.27	1.62	1.43	1.33	1.16	1.08
IV total	4.01	4.01	4.01	4.02	4.00	4.01	4.01	4.00	4.01	4.02	4.02	4.03
Fe	0.01	0.00	0.00	0.00	0.00	0.01	0.01	0.01	0.00	0.01	0.01	0.00
Mg	0.00	0.00	0.00	0.00	0.00	0.00	0.00	0.00	0.00	0.00	0.00	0.00
Ca	0.53	0.50	0.58	0.28	0.64	0.43	0.24	0.61	0.42	0.30	0.15	0.04
Na	0.44	0.48	0.40	0.66	0.34	0.53	0.70	0.37	0.54	0.64	0.77	0.87
K	0.00	0.00	0.00	0.00	0.00	0.00	0.00	0.00	0.00	0.02	0.01	0.01
VI total	0.98	0.99	0.99	0.95	0.99	0.98	0.96	0.98	0.96	0.96	0.94	0.92
An%	55	51	59	30	65	45	26	62	44	31	16	5

Table 4 (continued).

Sample number:	118-735B-58R-1 (Piece 10, 47–51 cm)			118-735B-63R-6 (Piece 5A, 94–98 cm)		118-735B-70R-1 (Piece 2B, 39–49 cm)		118-735B-81R-2 (Piece 1C, 23–31 cm)			
	Relict igneous	Alteration	Veinlet	Calcic igneous	Vein	Calcic igneous	Vein	Calcic igneous	Adjacent to green amph	Vein	Vein
SiO ₂	52.82	58.65	66.25	52.06	63.91	51.19	65.12	53.64	61.05	65.33	68.59
Al ₂ O ₃	30.56	26.88	21.56	31.00	23.38	31.38	22.42	29.93	24.99	21.48	20.33
Fe ₂ O ₃	0.24	0.16	0.18	0.33	0.00	0.34	0.11	0.14	0.11	0.09	0.01
MgO	0.03	0.00	0.00	0.02	0.00	0.02	0.01	0.00	0.01	0.00	0.01
CaO	12.81	8.17	2.19	13.13	3.96	13.63	2.76	11.93	6.07	2.24	0.29
Na ₂ O	4.22	6.58	9.65	4.04	8.74	3.70	9.75	4.53	7.61	9.40	10.66
K ₂ O	0.07	0.05	0.19	0.00	0.04	0.06	0.04	0.04	0.14	0.09	0.02
Total	100.74	100.47	100.03	100.58	100.01	100.31	100.20	100.22	99.96	98.63	99.91
Atoms based on 8 oxygens											
Si	2.38	2.60	2.90	2.35	2.81	2.32	2.86	2.42	2.71	2.90	2.99
Al	1.62	1.41	1.11	1.65	1.21	1.68	1.16	1.59	1.31	1.12	1.04
IV total	4.00	4.01	4.02	4.00	4.02	4.00	4.01	4.01	4.01	4.02	4.03
Fe	0.01	0.01	0.01	0.01	0.00	0.01	0.00	0.01	0.00	0.00	0.00
Mg	0.00	0.00	0.00	0.00	0.00	0.00	0.00	0.00	0.00	0.00	0.00
Ca	0.62	0.39	0.10	0.64	0.19	0.66	0.13	0.58	0.29	0.11	0.01
Na	0.37	0.57	0.82	0.35	0.75	0.33	0.83	0.40	0.65	0.81	0.90
K	0.00	0.00	0.01	0.00	0.00	0.00	0.00	0.00	0.01	0.01	0.00
VI total	1.00	0.96	0.94	1.00	0.93	1.00	0.97	0.98	0.95	0.92	0.92
An%	62	41	11	64	20	67	14	59	30	12	1

vapor with only a small amount of liquid. In rare cases, inclusions reach very large size (to 100 μm). Specific examples of inclusions in plagioclase are described below.

Quartz is rare in Hole 735B; it occurs in trondhjemite and in some veins associated with zircon, apatite, and diopside. In the trondhjemite, quartz contains sparse liquid plus vapor fluid inclusions up to about 10 μm across.

Hornblende often contains a few fluid inclusions that are thin long tubes oriented parallel to the *c*-axis. Typical dimensions are 1 to 5 μm wide and several tens of micrometers long. Vapor-to-liquid ratios vary considerably, suggesting that if the fluid inclusions are primary, then many of them have leaked subsequently owing to the excellent hornblende cleavage.

Thus, homogenization temperatures from hornblendes are suspect, but the fluid type (aqueous, types of salt, etc.) can still be evaluated.

Diopside that occurs in leucocratic plagioclase-diopside veins often contains abundant fluid inclusions. As in the hornblende, diopside-hosted inclusions are long and thin, oriented crystallographically, and homogenization temperatures must be evaluated critically because of the possibility of leakage along the cleavage.

Fluid inclusions have been observed in apatite in petrographic thin sections; however, no suitable material for fluid inclusion analyses has yet been obtained. Detailed fluid inclusion studies were performed on six samples using heating and

Table 5. Representative analyses of secondary minerals.

Sample number:	118-735B-45R-4 (Piece 7, 136–140 cm)						118-735B-54R-2 (Piece 1C, 32–40 cm)		118-735B-58R-1 (Piece 10, 47–51 cm)			
	Chlorite	Chlorite	Epid	Phlog	Analcime	Diop	Biotite	Biotite	Clinozois	Chlorite	Thomson	Prehnite
SiO ₂	27.99	22.87	38.18	37.43	56.64	52.13	34.67	37.45	39.44	27.34	41.60	43.55
TiO ₂	0.02	0.00	0.12	0.02	0.00	0.06	3.55	2.62	0.06	0.01	nd	nd
Al ₂ O ₃	17.62	19.28	29.01	19.93	25.32	0.22	13.03	9.48	32.80	20.29	30.04	24.64
FeO*	28.96	41.27		11.99	0.07	9.56	31.40	33.42		19.15	0.00	
Fe ₂ O ₃ **			6.67						2.47			0.20
MnO	0.46	0.46	0.07	0.14	0.00	0.28	0.13	0.31	0.00	0.55	nd	nd
MgO	12.53	4.43	0.02	18.77	0.00	13.43	4.54	5.03	0.06	20.58	0.00	0.05
CaO	1.08	0.03	24.44	0.02	0.13	24.27	0.00	0.56	23.49	0.06	11.48	27.22
Na ₂ O	0.03	0.04	0.02	1.53	13.38	0.27	0.10	0.11	0.01	0.01	3.77	0.14
K ₂ O	0.04	0.03	0.01	7.17	0.10	0.00	9.30	6.60	0.00	0.00	0.00	0.00
Cl	0.01	0.00	0.00	0.01	0.00	0.00	0.29	0.20	0.00	0.00	nd	nd
Total	88.72	88.41	98.52	97.01	95.63	100.21	97.01	95.78	98.34	87.97	86.88	95.79
#Oxy	28	28	25	22	6.5	6	22	22	25	28	23	22
Si	5.953	5.273	5.977	5.336	2.150	1.964	5.573	6.049	6.001	5.556	6.285	5.968
Ti	0.003	0.000	0.014	0.002	0.000	0.002	0.429	0.318	0.007	0.002	nd	nd
Al	4.416	5.240	5.353	3.349	1.133	0.010	2.468	1.804	5.883	4.860	5.348	3.988
Fe	5.151	7.958	0.873	1.429	0.002	0.301	4.221	4.514	0.315	3.254	0.000	0.018
Mn	0.082	0.090	0.009	0.017	0.000	0.009	0.018	0.042	0.000	0.094	nd	nd
Mg	3.971	1.521	0.004	3.988	0.000	0.754	1.088	1.210	0.014	6.233	0.000	0.011
Ca	0.246	0.007	4.099	0.003	0.005	0.980	0.000	0.097	3.829	0.012	1.857	4.015
Na	0.013	0.016	0.005	0.423	0.984	0.020	0.032	0.034	0.002	0.002	1.104	0.037
K	0.011	0.010	0.001	1.304	0.005	0.000	1.907	1.360	0.000	0.000	0.000	0.000
Cl	0.002	0.001	0.000	0.003	0.000	0.000	0.078	0.055	0.001	0.000	nd	nd
Total	19.848	20.116	16.335	15.854	4.279	4.040	15.813	15.483	16.052	20.014	14.594	14.036
Fe#	56.47	83.95		26.38			79.51	78.86		34.30		
Ps%			14.02						5.09			

Notes: * = Total iron as FeO; ** = Total iron as Fe₂O₃; mineral abbreviations: Epid = epidote, Phlog = phlogopite; Diop = diopside, Clinozois = clinozoisite, Thomson = thomsonite.

freezing techniques, and on 10 samples using nondestructive laser Raman spectroscopy. Tables of fluid inclusion data are available from D. Vanko. Summary results are presented next.

Veined Mylonitic Metagabbro

Sample 118-735B-2D-2 (Piece 6, 36–39 cm) is the veined metagabbro with mylonitic texture, containing labradorite and a range of aluminous hornblendes, with some actinolite and secondary apatite (Table 1). Data were collected from fluid inclusions in both plagioclase and hornblende. The plagioclase-hosted inclusions are generally small (5 to 10 μm) and irregular and form groups that are typically arrayed along healed fractures; thus, they should be classified as secondary. Some inclusions appear to contain one or more birefringent daughter crystals. Hornblende inclusions are long and tubular, and of varying liquid-to-vapor ratio. Some have a birefringent daughter crystal.

On freezing, inclusions in plagioclase and hornblende behave similarly: final ice melting occurs between -25° and -1.9°C , with modes at about -3° and -24°C (Fig. 15). These values indicate that fluid salinities vary considerably and that at least two generations of fluid are represented, with modes at 5 and >23 wt% NaCl equivalent. Some inclusions in plagioclase, notably those that appear to be vapor-rich, also form a clathrate compound upon freezing. Clathrate melting temperatures were measured at $+10.9^\circ$, $+22.2^\circ$, and $+25.3^\circ\text{C}$, which indicates the presence of methane.

Fluid inclusions generally homogenize at temperatures between 200° and 250°C (Fig. 16). Some hornblende inclusions remain unhomogenized at 500°C ; however, these are large tubes that most likely have leaked since trapping, forcing the homogenization temperature upward. Neglecting

these, most inclusions in plagioclase and hornblende behave similarly on heating. There is no correlation between ice melting and homogenization temperatures.

Fluid inclusion data suggest that the metamorphism of this sample, involving hydration and mylonitic deformation followed by minor retrograde alteration (e.g., minor actinolite), occurred with one of two possible fluids present: an aqueous fluid of locally (or temporally) variable salinity, or a methane-bearing aqueous solution. Homogenization temperatures (with a mode near 240°C) are very low relative to the inferred amphibolite-grade metamorphism ($>600^\circ\text{C}$, see below), and are probably related to the retrograde greenschist-facies alteration, during which inclusions were re-equilibrated and trapped.

Veined Metagabbro

Sample 118-735B-58R-1 (Piece 10, 47–51 cm) is an altered metagabbro from Unit V with a secondary assemblage that includes clinozoisite, prehnite, thomsonite, titanite, hornblende, actinolite, tremolite, chlorite, andesine, oligoclase, and albite. Remarkably, igneous labradorite having original dense, tiny, opaque inclusions still persists as relict cores. However, cutting these relict cores are diffuse veins of more sodic plagioclase where opaque inclusions have been removed during recrystallization. These zones contain abundant secondary fluid inclusions with two and three phases at room temperature. Some planes of inclusions are dominantly vapor, whereas other planes are mostly liquid. Birefringent daughter crystals are present in some cases, and other inclusions (particularly large ones that reach 100 μm wide) contain a small opaque daughter crystal having a hexagonal tabular shape.

Table 5 (continued).

Sample number:	118-735B-70R-1 (Piece 2B, 39-49 cm)				
	Chlorite	Chlorite	Clinozois	Diop	Augite
SiO ₂	26.32	26.02	38.59	53.42	51.75
TiO ₂	0.00	0.00	0.02	0.00	0.97
Al ₂ O ₃	21.14	20.61	32.67	0.23	3.34
FeO	15.92	24.84	2.86	7.67	6.37
Fe ₂ O ₃					
MnO	0.25	1.01	0.63	0.06	0.19
MgO	23.61	16.11	0.05	13.58	15.68
CaO	0.04	0.04	23.50	24.56	21.11
Na ₂ O	0.03	0.02	0.01	0.13	0.39
K ₂ O	0.00	0.00	0.00	0.00	0.00
Cl	0.00	0.02	0.00	0.00	0.00
Total	87.31	88.66	98.33	99.66	99.79
#Oxy	28	28	25	6	6
Si	5.310	5.431	5.914	1.998	1.908
Ti	0.000	0.000	0.002	0.000	0.027
Al	5.027	0.068	5.900	0.010	0.145
Fe	2.686	4.334	0.366	0.240	0.196
Mn	0.043	0.179	0.082	0.002	0.006
Mg	7.099	5.011	0.011	0.757	0.862
Ca	0.007	0.009	3.859	0.984	0.834
Na	0.010	0.007	0.002	0.010	0.028
K	0.001	0.000	0.000	0.000	0.000
Cl	0.001	0.006	0.000	0.000	0.000
Total	20.183	20.044	16.136	4.001	4.006
Fe#	27.45	46.38			
Ps%			5.85		

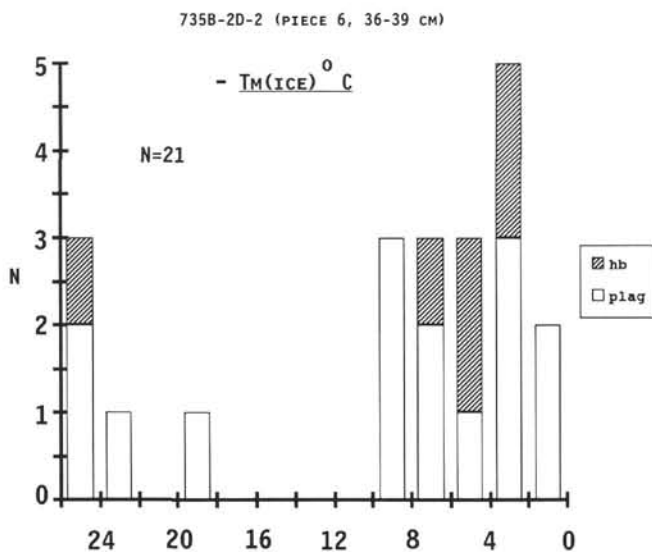


Figure 15. Histogram of ice melting temperatures of fluid inclusions in plagioclase and hornblende, veined mylonitic metagabbro. Note the wide apparent range in salinities (because salinity is proportional to $-T_m(\text{ice})$).

Freezing data (Fig. 17) show that fluids have ice melting temperatures between -0.4° and -2.7°C , with a single mode near -0.9°C , indicating about 1.6 wt% NaCl equivalent fluid. In vapor-rich inclusions, a clathrate typically forms upon freezing, with melting temperatures ranging from $+2.2^\circ$ to $+6.1^\circ\text{C}$. Observation of two very large inclusions at

735B-2D-2 (PIECE 6, 36-39 CM)

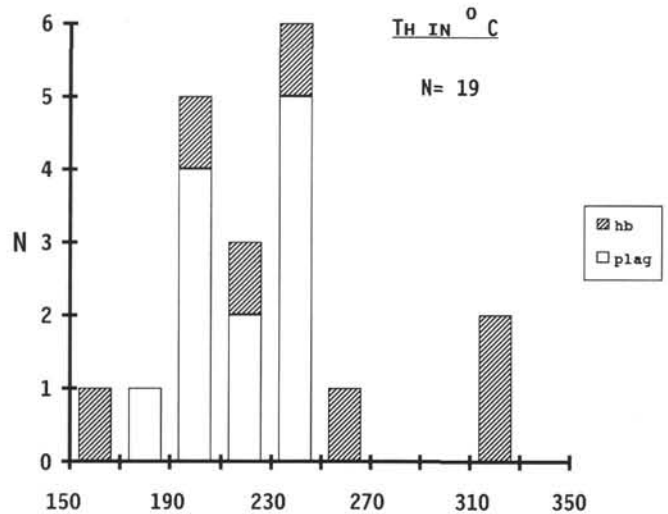


Figure 16. Histogram of homogenization temperatures of fluid inclusions in the veined mylonitic metagabbro. Two inclusions in hornblende that were unhomogenized at 500°C are not shown—they probably have leaked since trapping.

735B-58R-1 (PIECE 10, 47-51 CM)

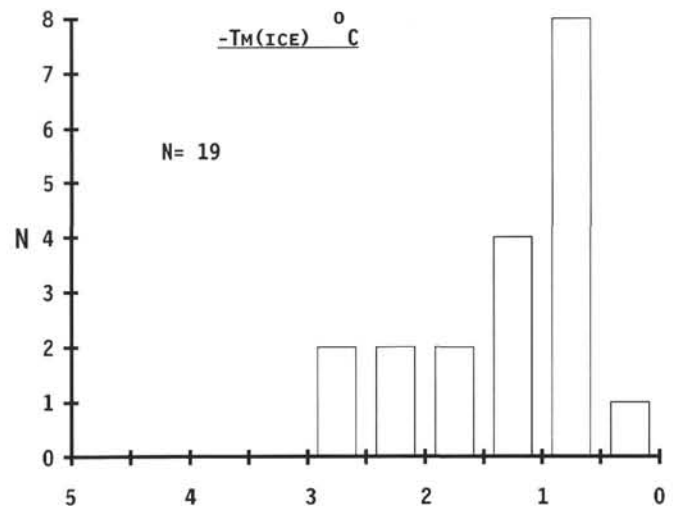


Figure 17. Ice melting temperatures from plagioclase inclusions in veined metagabbro. Note that salinity is relatively low (seawater has ice melting of about -2.1°C).

cryogenic temperatures shows a distinct melting event at $-182.5^\circ \pm$ about 2°C , which corresponds to the melting temperature of methane ice. No phase transitions at higher temperatures that could be explained by the presence of carbon dioxide were observed. Inclusions with clathrates have higher ice melting temperatures (-0.7° to -0.4°C , or about 1 ± 0.3 wt% NaCl equivalent) than inclusions without clathrates.

On heating, inclusions homogenize to liquid between 262° and 354°C (Fig. 18). However, there is a noticeable difference

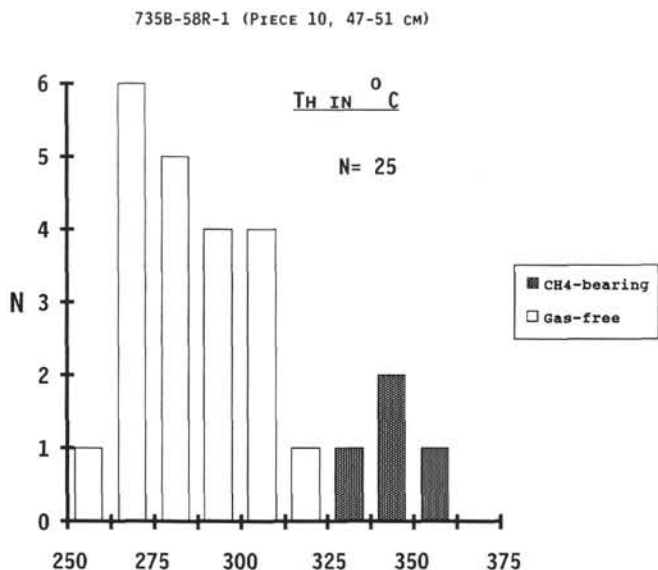


Figure 18. Homogenization temperatures of inclusions in plagioclase, veined metagabbro. Note that methane-bearing inclusions homogenize at a higher temperature.

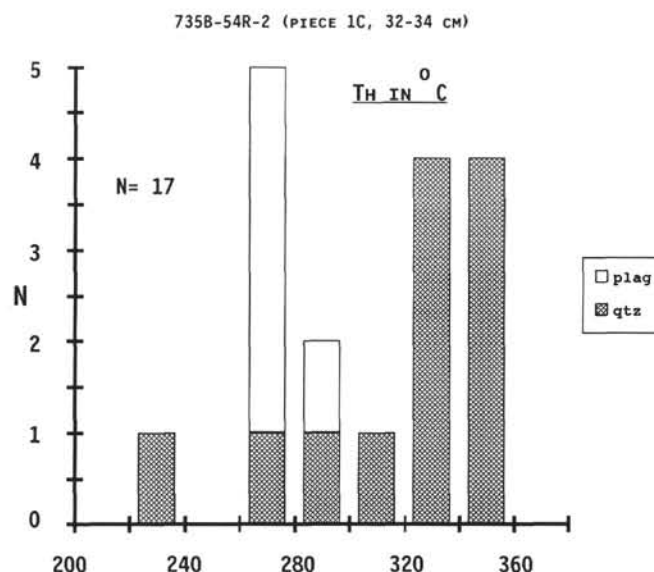


Figure 20. Homogenization temperatures from the trondhjemite sample. Inclusions in quartz tend to homogenize at higher temperatures.

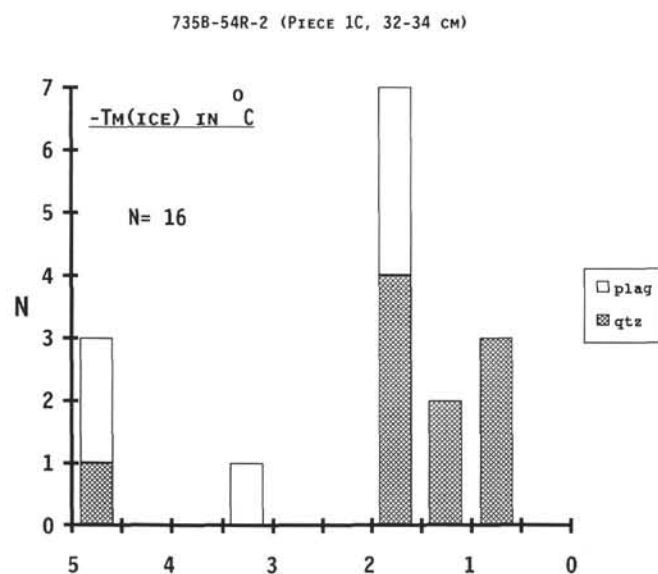


Figure 19. Ice melting temperatures from plagioclase and quartz inclusions, trondhjemite sample. Inclusions in quartz tend to contain slightly less saline fluid.

in T_h between liquid-rich (with a T_h mode around 270°C) and gas-rich (T_h mode of 345°C) inclusions.

Several small samples with inclusions were crushed during microscopic observation. In all cases, fluid inclusions exhibited vapor expansion when they were broken open, indicating the presence of compressed gas. Thermometric data indicate that this gas is methane, which was confirmed using laser Raman microspectroscopy (see section below).

Trondhjemite

Sample 118-735B-54R-2 (Piece 1C, 32-34 cm), the trondhjemite, contains sparse fluid inclusions in quartz and plagioclase. Those in quartz are vapor-rich, two-phase, often with

equant and negative crystal shapes, and oriented in clusters or along healed fractures. Those in plagioclase are more irregular, often flat or tubular, and two-phase at room temperature.

Freezing measurements show that ice melting occurs between -0.8° and -4.5°C , with most occurring at about -1.5°C (Fig. 19). Clathrate melting was observed in both quartz and plagioclase, with temperatures between $+1.6^\circ$ and $+7.1^\circ\text{C}$. The clathrates, together with some crushing tests performed on small plagioclase chips, show that a compressible gas is present in most inclusions. Although no observations were made at cryogenic temperatures, laser Raman work shows that the gas is methane (see section below).

On heating, inclusions in plagioclase homogenize at around $270^\circ \pm 10^\circ\text{C}$, and those in quartz homogenize (to liquid) between 227° and 358°C with a mode near 340°C (Fig. 20).

Leucocratic Diopside-Bearing Veins

Fluid inclusions in diopside from three leucocratic veins (Samples 118-735B-40R-3 [Piece 3A, 34-39 cm], 118-735B-63R-6 [Piece 5A, 94-98 cm], and 118-735B-70R-1 [Piece 2B, 39-49 cm]) were investigated. The fluid inclusions are typically tubular in shape, with about half liquid and half vapor (Fig. 11). Some inclusions, however, are larger (to about 15 or 20 μm) and irregular or equant in shape. In two of the samples, several inclusions in plagioclase also were studied. The plagioclase inclusions are two-phase equant to irregular inclusions, probably secondary in origin. In contrast, the inclusions in diopside could be primary.

Freezing temperatures show that the fluids in plagioclase and diopside are distinct. In Sample 118-735B-63R-6 (Piece 5A, 94-98 cm), $T_m(\text{ice})$ in plagioclase is from -0.1° to -0.9°C (0.2-1.6 wt% NaCl equiv) and $T_m(\text{ice})$ in diopside is from -1.2° to -2.2°C (2.1-3.7 wt% NaCl equiv) (Fig. 21). One inclusion in plagioclase had $T_m(\text{ice})$ at -17.8°C (21.0 wt% NaCl equiv). In Sample 118-735B-40R-3 (Piece 3A, 34-39 cm), plagioclase inclusions melt between -0.9° and -2.0°C (1.6-3.4 wt% NaCl equiv), and diopside inclusions melt between -1.7° and -2.7°C (2.9-4.5 wt% NaCl equiv) (Fig. 22). Consequently, fluids in diopside are slightly more saline than those in plagioclase. No inclusions in these samples gave any indication of the presence of clathrate or condensed gases at low temperatures.

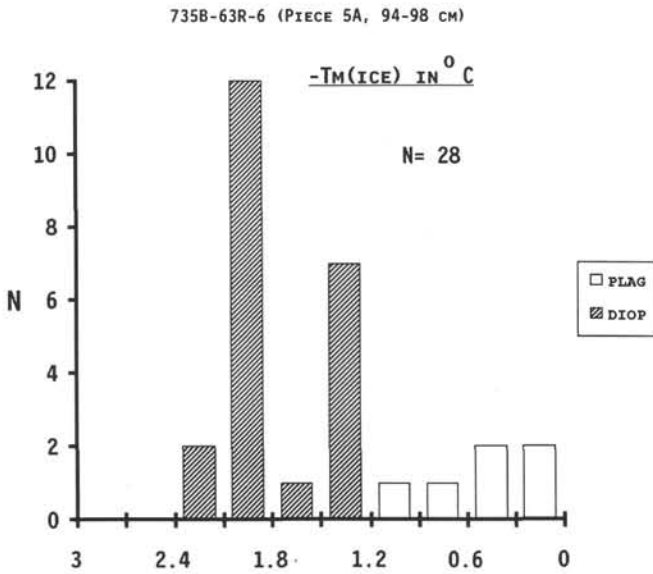


Figure 21. Ice melting temperatures from a leucocratic diopside-bearing vein. Fluids in diopside are distinctly more saline than those in plagioclase.

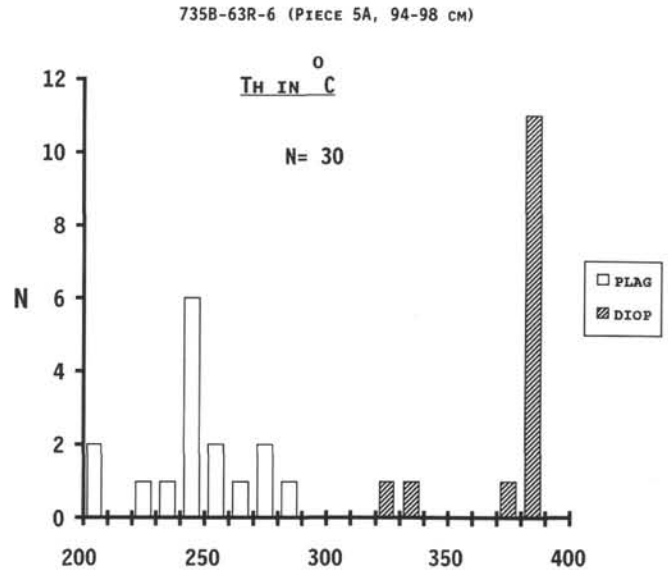


Figure 23. Homogenization temperatures from a diopside-bearing vein. Fluid inclusions in diopside homogenize at a higher temperature than those in plagioclase.

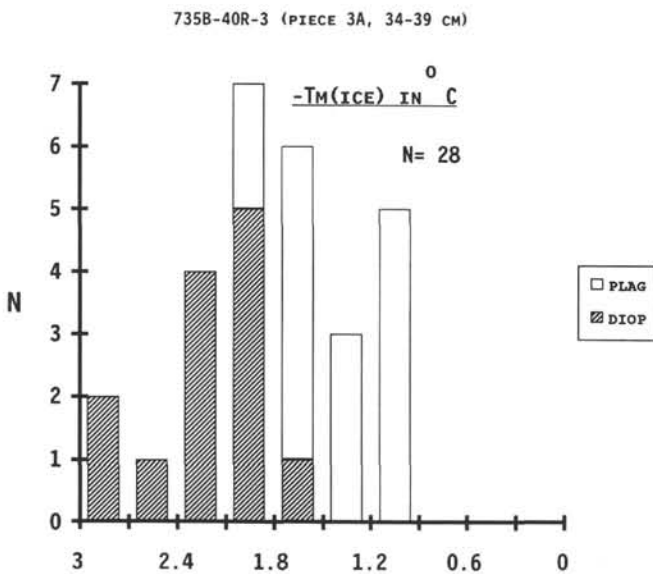


Figure 22. Ice melting temperatures from a second diopside-bearing vein. As seen in Figure 21, fluids in diopside are more saline than those in plagioclase.

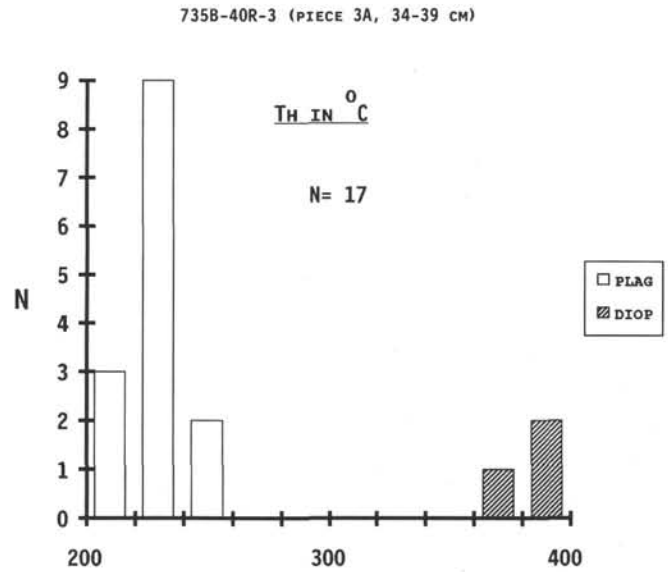


Figure 24. Homogenization temperatures from a second diopside-bearing vein, showing the same relationship as in Figure 23.

On heating, inclusions in plagioclase and diopside again behave differently. In Sample 118-735B-63R-6 (Piece 5A, 94-98 cm), plagioclase inclusions homogenize to liquid between 207° and 285°C, whereas diopside inclusions homogenize to liquid between 321° and 386°C, with a strong mode near 380°C (Fig. 23). In Sample 118-735B-40R-3 (Piece 3A, 34-39 cm), plagioclase inclusions homogenize to liquid between 213° and 242°C, and diopside inclusions homogenize variably to liquid or vapor between about 363° and 395°C (Fig. 24). Diopside inclusions in Sample 118-735B-70R-1 (Piece 2B, 39-49 cm) homogenize between 399° and 420°C to vapor (one inclusion homogenized with critical behavior and one homogenization was to liquid at 313°C) (Fig. 25). Apparently, the fluid inclusion populations pre-

served in plagioclase and diopside are distinct. Plagioclase inclusions are less saline and homogenize at lower temperature, and diopside inclusions are slightly more saline and homogenize at significantly higher temperatures. The inclusions in diopside may be primary and those in plagioclase may all be secondary.

Laser Raman Spectroscopy

Fluid inclusion contents were studied in 10 samples with a laser Raman microprobe to test for the presence of various Raman-active gases and compounds. The mylonitic metagabbro, Sample 118-735B-2D-2 (Piece 6, 36-39 cm), gave no Raman spectrum for any gas, even though microthermometric data clearly indicate that methane is present in some

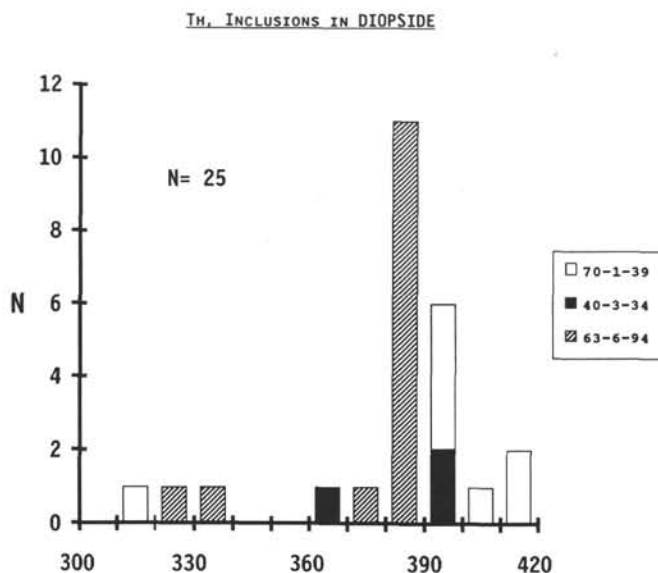


Figure 25. Summary of homogenization temperatures of inclusions in diopside for three leucocratic veins.

inclusions. A spectrum corresponding to calcite was obtained from a birefringent daughter crystal in plagioclase.

Of four metagabbros studied (Samples 118-735B-22R-3 [Piece 5A, 112–115 cm], 118-735B-25R-1 [Piece 3, 12–17 cm], 118-735B-26R-2 [Piece 2A, 8–12 cm], and 118-735B-58R-1 [Piece 10, 47–51 cm]), three contained abundant evidence of methane in plagioclase inclusions. Only Sample 118-735B-22R-3 (Piece 5A, 112–115 cm) failed to yield a methane signal. In one Sample (118-735B-25R-1 [Piece 3, 12–17 cm]), the methane-bearing inclusions were restricted to individual healed fractures, and other inclusions showed no signal. Some large fluid inclusions visible in Sample 118-735B-58R-1 (Piece 10, 47–51 cm) contain an opaque hexagonal platelet daughter crystal. These were tested by laser Raman for peaks characteristic of hematite and graphite, but without success. Optically and morphologically, however, graphite is the best candidate. In reflected light (albeit, focused within a fluid inclusion), the color was gray rather than reddish or yellowish.

The trondhjemite sample gave a strong methane signal for inclusions in quartz, but not in plagioclase. Four leucocratic diopside-bearing veins (those listed above, plus Sample 118-735B-41R-3 [Piece 4, 67–71 cm]) gave no signal for methane in the diopside inclusions.

The location of the major methane peak in a Raman spectrum is pressure-sensitive (Wopenka et al., 1990), as is the melting temperature of the methane clathrate (Mullis, 1979). Presumably, one could study these two independent pressure indicators further. We have not done this, because the pressures are not meaningful from a petrologic standpoint. Large inclusions in plagioclase, which are those most likely to have stretched or leaked, give the lowest methane clathrate melting temperatures (corresponding to low partial pressure of methane). The smallest plagioclase inclusions yield the highest clathrate melting temperatures (corresponding to higher internal pressures). Apparently, methane-bearing plagioclase inclusions are prone to leakage, thus no present internal pressures can be trusted to represent original pressures (corrected for cooling to room temperature).

Stable Isotopes

Downcore Profile of Whole-Rock Powders

Whole-rock powders of 94 samples from Hole 735B were produced on the *JOIDES Resolution* for shipboard XRF analyses, and their chemical compositions are listed in Site 735 chapter (Shipboard Scientific Party, 1989). Subsamples of these powders were analyzed for oxygen isotopes to establish a first-order downcore profile. This profile and its relationship to deformation and fluid penetration is discussed in Stakes et al. (this volume) and is only summarized here. Values of $\delta^{18}\text{O}$ for the whole-rock powders varied from 2.9 to 7.0, with more than one-half of the core being depleted in ^{18}O from a fresh mid-ocean ridge basalt δ value of 5.8‰ (Taylor, 1977; Stakes and O'Neil, 1982).

The upper 200 m (Units I and II) of the core has been pervasively depleted in ^{18}O due to interactions with seawater ($\delta = 0\text{‰}$) at temperatures in excess of 300°C. In this portion of the core, the greatest depletion of ^{18}O is associated with samples that are rich in chlorite and tremolite/talc formed during advanced coronitic replacement of olivine and plagioclase. These are samples for which the vein network and hydrous replacement of primary phases is most extensive. This relationship suggests that the whole rock $\delta^{18}\text{O}$ was controlled by the water/rock ratio, rather than by temperature variations.

Units III, IV and V have short zones of unaltered gabbro with primary compositions ranging from 5.5 to 6.2‰ as a function of modal proportions. The trondhjemite in Cores 118-735B-53R to 118-735B-57R has a slightly heavier $\delta^{18}\text{O}$ value near 7‰, which is normal for rocks of granitic compositions. The correspondence between major shear zones and depletion in ^{18}O indicates that the listric normal faults acted as conduits for fresh seawater during the final, brittle phase of deformation (Cannat et al., this volume; Stakes, et al., this volume). Less seawater penetrated to the lowermost shear zone, and zones of ^{18}O depletion associated with the ductile deformation are more restricted in the lower parts of the core. The large hydrothermal breccia zones in Unit V are strongly depleted in ^{18}O , reflecting the greater permeability of these zones compared to the shear zones.

Mineral Separates

Oxygen isotopic compositions of plagioclase, diopside, augite, and hornblende separates have been completed for 24 samples (Table 6). Augite porphyroclasts in metagabbros retain their magmatic oxygen isotopic composition, ranging from 5.08 to 5.4‰. Magmatic augite may have been pseudomorphed by actinolitic hornblende or actinolite with $\delta^{18}\text{O}$ values as low as 1.6‰. Augite and plagioclase separates were obtained from two metagabbro samples (118-735B-26R-2, [Piece 2A, 8–12 cm]; 118-735B-41R-1 [Piece 2B, 42–50 cm]). For both of these samples, plagioclase is isotopically depleted compared to augite, which is the inverse of normal magmatic compositions (Taylor, 1968). This apparent isotopic disequilibrium results from the facile isotopic exchange of plagioclase compared to the pyroxene and is the most sensitive indicator of high-temperature seawater interactions (Taylor, 1968; 1977).

Plagioclase separates have been obtained for 21 samples and range in isotopic composition from 6.8 to 2.1‰, with an average of 4.5‰. At equilibrium, igneous plagioclase should be about 0.5‰ more enriched than the coexisting igneous pyroxene, suggesting a δ value for fresh plagioclase of 5.6 to 6.0‰. The veined mylonitic gabbro sample (118-735B-2D-2, [Piece 6, 36–39 cm]) has a plagioclase $\delta^{18}\text{O}$ value (5.1‰) only

Table 6. Oxygen isotopic results from mineral separates and temperature calculations.*

Core, section, interval (cm)	Piece	$\delta^{18}\text{O}$ (WR or mineral)					Temperature ($^{\circ}\text{C}$)			
		WR	PLAG	AMPH	DIOP	CPX	water = 0	2	3	3.8
118-735B-										
2D-2, 36-39	6		5.12	3.69						
15R-1, 90-93	7B	4.22	4.39				309	400	465	
18R-3, 5-8	1	3.16	3.2	1.63			358	480	575	
19R-1, 124-128	15A	3.75	3.41	2.89			349	464	552	
22R-1, 56-62	7B			3.33						
22R-1, 142-147	17	3.32	3.88	2.96			328	431	507	
25R-1, 12-17	3		5.11 (Ca-plg)	1.91						
do, do	do		2.44 (Na-plg)				397	549	677	
26R-2, 8-12	2A		3.12	2.71		5.08	362	486	584	
31R-2, 100-104	4A	4.07	5.35 (vein)							
31R-3, 31-33	1D	3.61	3.52	5.28			344	456	540	
do, do	do		5.78 (vein)							
35R-6, 114-117	9C	4.25				5.4				
40R-2, 73-78	1I	4.2	5.59 (vein)							
41R-1, 42-50	2B	4.17	4.51	4.84						
53R-4, 5-15	1B	4.68	5.32	4.39			304	393	456	
55R-1, 59-69	4A	5.26	2.16							
57R-2, 11-18	1B	4.43	2.05	1.94			420	592	746	
57R-4, 0-6	1A		6.57 (vein)							
58R-3, 8-16	1A	4.38	3.83 (vein)	2.07			331	434	511	
63R-7, 80-87	11A	4.22	7.44 (vein)							
64R-3, 95-104	5C		4.12 (vein)				319	416	486	
70R-1, 39-49	2B		4.72 (vein)		2.67		297	382	442	503
72R-7, 42-47	3		4.71							
78R-3, 110-119	5D	6.63	6.84 (vein)							
81R-6, 87-90	5			5.2						

* Temperatures calculated assuming equilibrium between plagioclase An_{30} and water of the isotopic composition shown.

slightly depleted from what would be expected in a fresh gabbro, although later amphibole is much lighter (3.7‰). This is consistent with the deformation occurring under conditions of low water/rock ratio (see Stakes et al., this volume; Cannat et al., this volume). Sample 118-735B-25R-1 (Piece 3, 12-17 cm) contains two optically distinguishable generations of plagioclase. Early inclusion-charged calcic plagioclase porphyroclasts have a $\delta^{18}\text{O}$ value of 5.11‰, similar to that observed in the mylonite, suggesting only slight isotopic re-equilibration. Later-stage milky-white sodic plagioclase has a $\delta^{18}\text{O}$ value of 2.44‰, consistent with the influx of seawater at a minimum temperature of about 400°C (see temperature section below for further discussion) and timing that is contemporaneous with the green hornblende in cross-cutting veins ($\delta^{18}\text{O} = 1.91‰$). Sample 118-735B-26R-2 (Piece 2A, 8-12 cm) exhibits similar depletions in ^{18}O with a bulk plagioclase $\delta^{18}\text{O}$ of 3.1‰ and a green amphibole $\delta^{18}\text{O}$ of 2.7‰. The plagioclase from this sample must have been thoroughly exchanged to have such a low total value.

Several samples contain veins or apophyses of a late magmatic (trondhjemitic) liquid characterized by the presence of apatite, euhedral sodic plagioclase, diopside, zircon, biotite, and small amounts of quartz (Stakes et al., this volume). The largest concentration of these veins is near the trondhjemitic intrusion in Core 118-735B-54R, but small feldspathic intrusions were found throughout the core. Plagioclase in these zircon-bearing zones is usually near-magmatic in isotopic composition (e.g., Core 118-735B-81R), except in the highly brecciated zones where low-temperature minerals such as epidote and chlorite are abundant. The oxygen isotopic results for the feldspathic veins do not consistently indicate a magmatic origin for the plagioclase, suggesting that some of these late magmatic injections were also subjected to hydrothermal alteration. Samples 118-735B-31R-2 (Piece 4A, 100-104 cm), 118-735B-31R-3 (Piece 1D, 31-33 cm), 118-735B-40R-2 (Piece 1I, 73-78 cm), 118-

735B-53R-4 (Piece 1B, 5-15 cm), 118-735B-57R-4 (Piece 1A, 0-6 cm), 118-735B-63R-7 (Piece 11A, 80-87 cm), and 118-735B-78R-3 (Piece 5D, 110-119 cm) are examples for which the plagioclase is isotopically heavy, near magmatic compositions (Table 6). Plagioclase from Section 118-735B-63R-7, however, is much heavier than expected for a magmatic composition, and this is probably due to admixture of heavy prehnite and analcime in the mineral separate. For the samples from Sections 118-735B-63R-7, 118-735B-31R-2, and 118-735B-31R-3, the vein plagioclase is "magmatic" in ^{18}O composition, while the adjacent host rock exhibits significant hydrothermal alteration to lower values of $\delta^{18}\text{O}$.

Leucocratic diopside-plagioclase veins of hydrothermal origin (based on low-temperature minerals, fluid inclusions, and light oxygen isotopic values) have an unclear relation to the trondhjemitic-impregnated breccia horizons (Stakes et al., this volume). The best example is Sample 118-735B-70R-1 (Piece 2B, 39-49), which has sodic plagioclase ($\delta^{18}\text{O} = 4.72‰$) and diopside ($\delta^{18}\text{O} = 2.67‰$). Fluids having an isotopic composition similar to those responsible for the vein assemblages have also altered the gabbro adjacent to some of the breccia horizons. An example is Sample 118-735B-64R-4 (Piece 1H, 73-76 cm) in which the original plagioclase of An_{67} is cut by diopside veins. There is extensive secondary chlorite, epidote, sodic plagioclase (An_{44-20}) and actinolite (with no hornblende). A plagioclase vein from an adjacent sample has $\delta^{18}\text{O}$ of 4.12‰, suggesting that alteration was by a seawater-derived fluid.

DISCUSSION

Styles of Alteration

The 500 m of core recovered from Hole 735B exhibits several contrasting styles of alteration that are associated with various styles of deformation. Lithologic Units I and II

are dominated by a high-temperature hydration that resulted in hydrothermal metamorphism of the gabbros variably to foliated metagabbros and mylonitic gabbros. Abundant small veins, oriented at a high angle to foliation and containing primarily hornblende plus or minus intermediate plagioclase (andesine), were interpreted by Leg 118 shipboard scientists to represent infilling of small brittle fractures that formed during the termination of ductile deformation. The sense of strain indicated by both tiny veins and the metagabbroic foliation is identical (Shipboard Scientific Party, 1989), and our analyses show that the composition of "metamorphic" amphibole and plagioclase in the foliation and "hydrothermal" amphibole and plagioclase in the veinlets is commonly identical. In other cases, the amphiboles in high-angle veins vary to lower aluminum and alkali contents, sometimes in concert with plagioclase variation to more sodic compositions (e.g., Sample 118-735B-1D-1 [Piece 1, 0–5 cm] and 118-735B-25R-1 [Piece 3, 12–17 cm]).

A contrasting style of high-temperature hydrothermal veining is present in Units III, V, and VI (as well as the base of Unit II). Here, hydrothermal alteration is commonly concentrated around centimeter-scale leucocratic veins, which usually contain primary hydrothermal diopside. Host gabbro adjacent to the veins underwent variable minor alteration, with hydration of mafic phases and albite veining of the igneous labradorite. Some of these rocks also contain an intermediate plagioclase (andesine or oligoclase), suggesting that this albitization is just the last and lowest-temperature stage of a complex alteration history.

Brecciation, common at discrete horizons within Units IV, V, VI, and at the Unit II/III boundary, introduced a more pervasive localized hydrothermal solution that was responsible for extensive development of secondary minerals, such as chlorite, titanite, actinolite, albite, epidote, diopside, apatite, calcite, analcime, and thomsonite. The alteration near breccia zones is similar to that along the leucocratic veins.

Hydrous magmatic crystallization, characterized by widespread development of albite with accessory ferro-actinolitic hornblende, apatite, and halogen(Cl,F)-bearing biotite, is exhibited by the late-stage trondhjemite intrusion. The fluorine composition of biotite suggests that the hydrous crystallization here is deuteric or late magmatic, because seawater-type hydrothermal fluids are not expected to contain fluorine as well as chlorine.

The alteration assemblages observed in Hole 735B are similar in many respects to those in hydrothermal veins in the Skaergaard layered intrusion of East Greenland (Bird et al., 1986) and the Bushveld layered complex of South Africa (Schiffries and Skinner, 1987; Schiffries and Rye, 1990). In both these settings, early high-temperature veining took place under conditions similar to amphibolite-grade metamorphism, and subsequent veining occurred in greenschist and zeolite grade-equivalent conditions. The most notable difference between the continental intrusions and Hole 735B is that the layered intrusions are much less deformed, so that the ductile foliation and resulting metamorphic hydration inferred for Hole 735B has no analog in the layered intrusions.

Mineral chemistry aids when categorizing the contrasting alteration styles seen in Hole 735B. For example, vein amphibole chemistry of the upper two lithologic units is dominantly hornblende and alkali-rich hornblende (hastingsitic or pargasitic), whereas veins in the lower units have much more common actinolitic hornblendes and actinolites. Similarly, the upper two units tend to contain andesine as a secondary plagioclase, whereas the lower units contain oligoclase and albite as well.

The distribution of metamorphic and vein minerals and the style of deformation suggest that a boundary of sorts may be located at approximately Core 118-735B-30R, in the lower part of Unit II. This is the shallowest occurrence of hydrothermal diopside and also coincides roughly with the shallowest vein epidote (or clinozoisite) and titanite. Moreover, secondary plagioclase above this level is primarily oligoclase or andesine, whereas below this level it is more albitic. Roughly in concert with this change, hydrothermal veining in Units I and II is dominantly aluminous hornblende and plagioclase in tiny early veinlets, whereas alteration lower in the hole is associated with brecciated horizons or centimeter-scale leucocratic veins.

Another aspect of mineral chemistry that changes subtly downhole is the halogen composition of hydrated minerals. Chlorine contents of amphiboles in Units I, II, and III commonly reach several tenths of a percent and get as high as 1.5 wt%. In contrast, amphiboles from Units IV, V, and VI are typically chlorine-poor. Perhaps the higher-chlorine amphiboles attest to alteration under conditions of lower water-to-rock mass ratio (W/R), such that chlorine is concentrated first in the fluid phase, then as a result becomes concentrated in amphibole. The lower-chlorine amphibole associated with breccias and centimeter-scale veins might result from a situation where fluid flows more readily through permeable zones of brecciation, W/R is substantially higher, and therefore chlorine does not get concentrated. Limited fluid inclusion evidence is consistent with this idea: inclusions from Sample 118-735B-2D-2 (Piece 6, 36–39 cm) have variable salinity that reaches some very high values (near halite saturation), whereas most inclusions from centimeter-scale leucocratic veins contain normal salinity fluids (salinity from less than that of seawater to about two or three times seawater).

Alternate explanations for the variable salinities observed in fluid inclusions within Units I, II, and III are that (1) fluids underwent a phase separation, or (2) fluids of variable salinity actually have different origins (e.g., the high-salinity ones are magmatic whereas the lower salinity ones are hydrothermal). Based on the samples studied so far, there is no clear evidence for phase separation, such as the coexistence of appropriate conjugate fluid types. The inclusions exhibiting variable salinity are petrographically similar, hence an interpretation of one type as magmatic and another as hydrothermal is unwarranted. More samples must be analyzed to ascertain further systematics in the fluid inclusion compositions.

Chlorite compositions have been used to distinguish zones of seawater downflow and upflow (Mottl, 1983). In the downflow regime, seawater loses magnesium to clays and chlorite, and in the upflow regime, hydrothermal solutions are already devoid of magnesium, hence chlorites are iron-rich. Extending this idea, proposed for oceanic layer 2, into layer 3 does not work well. Chlorites in coronitic replacements of mafic igneous phases are magnesian, and vein or breccia chlorites are commonly iron-rich. However, chlorites in some altered samples are highly variable in Fe-number, even within a single interstitial patch (Table 5). This is probably because of a strong local mineralogic control on secondary chlorites.

Fluid Types

Clearly, seawater had an important role in the alteration observed in Hole 735B. The best proof that seawater was the main alteration agent is the diagnostic shift in oxygen isotopes to low values. This was effected at temperatures greater than 300°C by a modified seawater solution (see below). Supporting

(but not conclusive) evidence for a seawater component to the alteration is found in the chlorine-bearing amphibole compositions and the saline nature of fluid inclusions in secondary minerals.

Seawater was important as the source of hydration of gabbros in Units I and II, where the W/R ratio was apparently very low and the modified seawater became moderately saline. Seawater also was the source of much of the hydration associated with local zones of brecciation and leucocratic veining within Units III, V, VI, and the base of II, but the W/R ratio there was higher, fluid flowed through more efficiently, and solutions did not readily become very saline.

A surprising feature of many fluid inclusions studied from Hole 735B is the presence of methane in the saline aqueous fluid. Methane was discovered in secondary inclusions within metagabbro labradorite, in primary inclusions within secondary intermediate-plagioclase veinlets cutting labradorite, and in secondary inclusions within trondhjemite quartz. Thus, this gas was apparently widespread, both at the time of hydrothermal metamorphism and of trondhjemite intrusion, but was not ubiquitous. No other gases were detected: in particular, no carbon dioxide was found. If the opaque daughter crystals in some methane-bearing inclusions are graphite, then the fluids can be categorized as slightly saline, aqueous, methane-bearing fluids having extremely low oxygen fugacity.

One possible source of methane is as a magmatic gas. Oceanic basalts contain dissolved gases that are dominated by water and carbon dioxide (e.g., Delaney et al., 1978; Muenow et al., 1980), although traces of methane and carbon monoxide have been detected in some mid-ocean ridge basalts (MORB) (Byers et al., 1983; 1986). The total lack of detectable carbon dioxide in Hole 735B inclusions suggests that these oceanic gabbros had very little interaction with normal MORB-type magmatic fluids. If methane is not a magmatic gas concentrated by fractionation processes, then it might have a source below this structural section, perhaps within the upper mantle. Although MORB magmatic gases have relatively high oxygen fugacity, primitive mantle material may have a somewhat lower oxygen fugacity (e.g., Christie et al., 1986; Wood and Virgo, 1989) that permits up to about 10% of any coexisting primitive mantle fluid to be methane (the rest being water and carbon dioxide). The methane observed in Hole 735B fluids may be comparable to the "mantle" methane characterized as such on the basis of primitive carbon isotopic abundances and observed as a trace constituent in modern black smoker fluids (Welhan and Craig, 1983; Welhan, 1988). Still, the lack of detectable carbon dioxide argues against an origin from primitive mantle fluids.

An alternative to primitive mantle methane is methane generated through serpentinization reactions within upper mantle ultramafic rocks. Hydration reactions between carbonate-bearing seawater (or modified seawater) and highly reduced mantle ultramafic rocks might reduce carbonate to methane (e.g., Frost, 1985; Abrajano et al., 1988). Janecky and Seyfried (1986) detected hydrogen and methane as by-products in some hydrothermal peridotite serpentinization experiments. Methane-rich gas seeps associated with serpentinized ultramafic rocks in the Philippines (Abrajano et al., 1988) may have formed by this mechanism.

If reduction of seawater carbonate to methane can take place during serpentinization of upper mantle ultramafic rocks, then a similar reduction might be possible in crustal cumulate ultramafic or mafic rocks. Thus, methane might be a natural by-product of layer 3 hydration and metamorphism under conditions of low water-to-rock ratio. Alt et al. (this volume) have proposed that the observed alteration of olivine

to a magnetite-bearing assemblage, at low W/R ratio, might generate significant H_2 . In the presence of carbonate or CO_2 , methane might then be expected to form.

Methane-bearing fluid inclusions have been reported from the Bushveld Intrusion, a large continental mafic intrusion (Schiffries, 1985). There, the origin of the methane also is not yet clear; however, a situation analogous to oceanic layer 3 is not unlikely.

Methane-bearing hydrothermal fluids may play an important role in deep crustal processes. Sustained low oxygen fugacity in the fluid phase may promote transport of those metals whose solubilities are higher when they are reduced (iron, for instance). Methane-bearing fluid inclusions also represent a new, albeit small, crustal reservoir for this gas, which may then be released into later hydrothermal fluids, or to fluids that are liberated as a crustal slab is eventually subducted.

Temperatures of Alteration

The Leg 118 shipboard scientists (Shipboard Scientific Party, 1989) recognized that temperatures of alteration were consistent with the equivalent of amphibolite facies conditions in the deformed and mylonitic metagabbros and with greenschist facies conditions in association with breccia horizons and leucocratic veins. Our mineral chemical data support this interpretation.

The results of geothermometric calculations based on hornblende and plagioclase compositions (Spear, 1980; Plyusnina, 1982) are listed in Table 7. The temperatures obtained have a probable uncertainty of $\pm 50^\circ C$. The Plyusnina (1982) method is based on experiments having a low-variance mineral assemblage, and none of our samples contained the complete assemblage (see notes, Table 7). Nonetheless, those rocks lacking only one or two minerals were used to estimate temperatures, and the results compare favorably with the Spear (1980) empirical geothermometer.

In some samples, the presence of only one or two hornblende types and one or two plagioclase types made the geothermometry straightforward. But in the more complex samples, having a range of hornblende and plagioclase compositions, the coexisting hornblende and plagioclase had to be chosen on the basis of prejudice—the more aluminous hornblendes were assumed to have coexisted with the more calcic plagioclases.

Results (Table 7) demonstrate that the metamorphic assemblages characteristic of Units I and II (i.e., metamorphic plagioclase and amphibole that defines the rock foliation) crystallized at amphibolite grade conditions, with temperatures of about 590° to $720^\circ C$ (most estimates are around $640^\circ C$). The high-temperature veining, which produced hornblende and plagioclase veins, took place with lowering temperature in the range of 640° (e.g., andesine [An_{41}]-bearing vein in Sample 118-735B-26R-2 [Piece 2A, 8–12 cm]) to $520^\circ C$ (e.g., andesine [An_{31}]-bearing vein in Sample 118-735B-12R-1 [Piece 5D, 65–68 cm]). Late-stage alteration involving albite and oligoclase, characteristic of the brecciated horizons, occurred at less than $500^\circ C$.

The trondhjemite intrusion recorded alteration at around 550° to less than $500^\circ C$. The sample with a diopside-bearing vein (Sample 118-735B-68R-3 [Piece 5, 62–64 cm]) records a metamorphic temperature of $710^\circ C$ in the host gabbro, but low temperatures of 505° to $480^\circ C$ related to the diopside veining.

Other secondary minerals associated with the late-stage oligoclase and albite alteration include titanite, chlorite, and iron-poor epidotes and prehnite. These phases typically occur in metabasic rocks at greenschist or transitional greenschist-to-amphibolite grade conditions. Titanite formed in 200 MPa

Table 7. Summary of plagioclase-hornblende temperature estimates.

Sample number	Minerals	Spear (1980)			Plyusnina (1982)			
		Ln(Ca,M4/Na,M4) in amphibole	Ln(XAn/XAb) in plagioclase	T (graphical)	wt% Al ₂ O ₃	T (graphical)	X An	T (graphical)
118-735B-1D-1 (Piece 1, 0–5 cm)	Mg-hast-hb with An ₄₆	2.69	–0.16	495				
	Mg-hb with An ₂₀	3.22	–1.39	480				
118-735B-2D-2 (Piece 6, 36–39 cm)	Mg-hast with An ₅₃	2.54	0.1	660				
	Mg-hb with An ₅₃	2.1	0.1	720				
118-735B-7D-1 (Piece 2A, 10–16 cm)	Mg-hast-hb with An ₄₅	2.3	–0.2	640				
	Mg-hb with An ₃₁	1.78–2.10	–0.8	530–550				
118-735B-12R-1 (Piece 5D, 65–68 cm)	Ed-hb with An ₃₁	2.7	–0.8	520				
	Mg-hb with An ₃₁	2.59	–0.8	525				
118-735B-14R-3 (Piece 2A, 31–35 cm)	Mg-hb with An ₄₉	2.26	–0.04	595				
118-735B-22R-3 (Piece 5A, 112–115 cm)	Tsch-hb with An ₂₉	1.77	–0.9	535				
	Mg-hb with An ₂₉	2.38	–0.9	520				
118-735B-25R-1 (Piece 3, 12–17 cm)	Mg-hb with An ₄₆	2.2	–0.16	640				
118-735B-26R-2 (Piece 2A, 8–12 cm)	Mg-hb with An ₄₃	1.98	–0.3	640				
118-735B-36R-1 (Piece 3, 17–20 cm)	Mg-hb with An ₃₈	2.34	–0.51	560				
118-735B-37R-2 (Piece 1H, 113–117 cm)	Mg-hst-hb, ed-hb, mg-hb; with An ₃₆	1.97–2.51	–0.6	530–590	8 to 11	550–630	34–37	540–550
	Act-hb with An ₂₁	2.28	–1.32	500	2 to 4	<450	21 to 15	510–500
	Act with An ₁₅	1.63–3.14	–1.73	<500				
118-735B-54R-2 (Piece 1C, 32–34 cm)	Fe-hb with An ₃₁	1.94	–0.8	550				
	Fe-act-hb with An ₁₀	1.87	–2.2	<490				
118-735B-58R-1 (Piece 10, 47–51 cm)	Tsch-hb with An ₃₁	2.28	–0.8	525	8.5 to 10.5	560–620	<31	<530
	Mg-hb with An ₂₃	1.55	–1.21	520				
	Act-hb with An ₁₁	2.82	–2.09	<490	5	470	>3	<500
118-735B-68R-3 (Piece 5, 62–64 cm)	Mg-hast with An ₅₂	2.18	0.08	710	15.3	>650		
	Act-hb with An ₁₉	2.55	–1.45	490	5.8	480	19	505
118-735B-87R-7 (Piece 1C, 15–17 cm)	Edenite with An ₂₅	2.28	–1.1	510				

Notes: The Plyusnina (1982) model is based on experiments involving hb, zoisite, plag, chlorite, calcite, and quartz, at $X(\text{CO}_2) = 0.1$, and $P = 2$ kb. None of the samples in this study contains all of these phases. Missing phases are: 37R-2-cc, qtz; 58R-1-chl, cc, qtz; 68R-3-cc, qtz. All temperatures given here are in degrees C, and are estimated to be good to $\pm 50^\circ\text{C}$. In those samples having a range of hornblende and plagioclase compositions, the more calcic plagioclases were paired with the more aluminous hornblendes when determining these temperatures.

(2 kb) experiments has a maximum thermal stability of about 500°C (e.g., Moody et al., 1983). Chlorite in those and similar experiments (Liou et al., 1974) persisted up to around 400° or 550°C, depending on whether oxygen fugacity was low or high, respectively. The chlorite in our samples is a relatively high-temperature type, based on the consistently high Al_2O_3 concentrations (Table 5, and see, e.g., Maruyama et al., 1983).

Experiments involving epidote and prehnite (e.g., Liou et al., 1983) demonstrate that these minerals coexist over a range of temperature, pressure, and oxygen fugacity and that their compositions vary systematically. Iron-rich epidote and prehnite solid solutions coexist up to about $350 \pm 30^\circ\text{C}$ at 100 MPa. Many epidotes from Hole 735B are iron-poor, and the prehnite that we have analyzed is also iron-poor. For example, in Sample 118-735B-58R-1 (Piece 10, 47–51 cm), the epidote mineral is a clinzoisite with 5 mol% pistacite component, and the prehnite has only 0.20 wt% Fe_2O_3 (Table 5). Liou et al. (1983) demonstrated that decreased iron in epidote and prehnite correlate with higher temperatures and lower oxygen fugacity. The distribution coefficient for iron and aluminum between epidote and prehnite also increases as a function of temperature, and the distribution coefficient calculated for our sample (from Section 118-735B-58R-1) is very high (13.4) compared to the range of K_{DS} (1.5 to 10.8) listed in Liou et al. (1983). Consequently, the temperature at which these two phases formed was probably somewhat higher than 350°, possibly 400°C or more.

The isotopic composition of secondary phases can also be used to estimate temperatures of formation. The mineral compositions depend not only on the temperatures of formation, but also on the isotopic composition of the fluid present. Seawater has an isotopic composition of zero, but may shift to higher values during interactions with crustal rocks at high temperatures, with the isotopic shift of the fluid depending on the ratio between the two reservoirs of ^{18}O —rocks and water. In addition, estimates of the temperatures of formation of plagioclase are dependent on the composition of the plagioclase (O'Neil and Taylor, 1967). We have calculated temperature estimates for plagioclase separates based on seawater (0‰) and isotopically shifted seawater (2, 3‰) for secondary andesine (An_{30}) (Table 6). The calculated temperatures are minima for two reasons: the calculation breaks down if the water-rock ratio is less than about unity (e.g., Stakes and O'Neil, 1982); and the mineral separates may contain small amounts of primary plagioclase, which should make the separate of secondary material seem less depleted and, consequently, the calculated temperature lower. Because of the first concern, temperatures were calculated only for vein plagioclase, not for megacrysts that may have had low W/R ratios. At W/R ratios less than one, the extent of isotopic depletion and the final isotopic composition of the plagioclase is limited by external fluid availability, thus, the final ^{18}O of plagioclase depends more on W/R ratio than on temperature.

Results of this approach show that calculated minimum temperatures range from about 300°C (with normal seawater) up to more than 600°C. These values coincide generally with the hornblende-plagioclase temperature estimates based on mineral chemistry discussed above.

Temperatures of mineral formation may be estimated on the basis of oxygen isotopic fractionation between coexisting minerals if the equilibrium fractionations have been calibrated in the laboratory. We attempted this technique with a leucocratic diopside-bearing vein (Sample 118-735B-70R-1 [Piece 2B, 39–49]), that contains sodic plagioclase ($\delta^{18}\text{O} = 4.72\text{‰}$) and diopside ($\delta^{18}\text{O} = 2.67\text{‰}$) (Table 6). The secondary plagioclase in this sample (An_{9-15}) has low-tem-

perature, low-salinity fluid inclusions, as well as minute inclusions of epidote, prehnite, and calcite, indicating that it has been retrograded. The diopside preserves primary high-salinity fluid inclusions and probably preserves an original isotopic value, as the low-temperature oxygen isotopic exchange in pyroxene is very sluggish and the diopside is mineralogically unaltered. We estimate the temperature of diopside-bearing veining to be 480° to 505°C (from plagioclase-amphibole thermometry). This estimate can be tested in light of the equilibrium diopside-plagioclase oxygen isotopic exchange (Matthews et al., 1983). Choosing an original plagioclase of An_{30} , and a temperature range of 480° to 505°C, the original plagioclase isotopic value in equilibrium with diopside ($\delta^{18}\text{O} = 2.67\text{‰}$) would be 4.88 to 4.74‰, matching closely the isotopic composition of the plagioclase separate. Subsequent albitization of that plagioclase at lower temperature (300° to 400°C) produced An_{10} , and if the water-rock ratio was very low, the isotopic composition of the original plagioclase may not have shifted appreciably during albitization.

The isotopic composition of the albite separate from the diopside-bearing vein (+4.72‰) is nearly equal to the expected composition of An_{30} in equilibrium with diopside (+2.67‰) and fluid at about 500°C. If we assume isotopic equilibrium, then the equation of Matthews et al. (1983) yields an equilibration temperature of 509°C. The isotopic composition of the fluid at these conditions can be calculated from either the diopside-water or plagioclase-water equilibrium fractionation: we obtain a value of +3.8‰ for that fluid, representing a substantial shift from seawater.

Pressure of Alteration

The trapping temperature of a primary fluid inclusion is higher than the experimental homogenization temperature: the magnitude of the difference is a function of the trapping pressure (Roedder, 1984). Therefore, given a measured homogenization temperature and an independent estimate of the temperature of mineral formation (in this case, from mineral

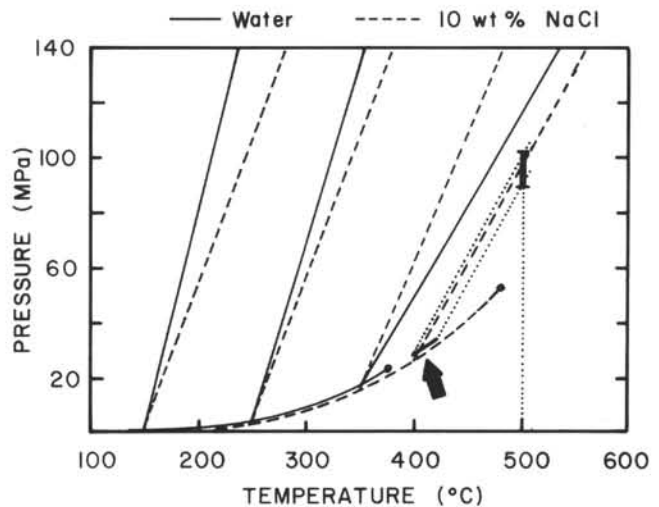


Figure 26. P-T plot for pure water and a 10 wt% NaCl solution showing the liquid-vapor curve terminating at a critical point (solid dots), and selected isochores (curves of constant specific volume) [after Roedder and Bodnar, (1980)]. Also shown are pressure constraints for 3.5 wt% NaCl fluid inclusions in diopside, Sample 118-735B-70R-1 (Piece 2B, 39–49 cm), which homogenized at $410 \pm 10^\circ\text{C}$ and which crystallized at about 500°C. The corresponding pressure limits are 90 to 100 MPa (0.9–1.0 kb).

geothermometry and oxygen isotopes), then the trapping pressure can be evaluated.

For the leucocratic diopside-bearing vein in Sample 118-735B-70R-1 (Piece 2B, 39–49 cm), primary fluid inclusions in diopside homogenize at $410^{\circ} \pm 10^{\circ}\text{C}$. The temperature of vein formation is estimated to be around 500°C . The fluids have a salinity of about 3.5 equivalent wt% NaCl (i.e., similar to seawater). As shown in Figure 26, the appropriate pressure adjustment that would rectify a $410^{\circ} \pm 10^{\circ}\text{C}$ homogenization with trapping at 500°C is 90 to 100 MPa (using the data compiled in Roedder and Bodnar [1980]). Under lithostatic load, which is probably more appropriate for layer 3 than hydrostatic load (Goldfarb and Delaney, 1988), this lithostatic pressure should be encountered at a depth of 1.7 to 2.0 km below a 4000-m-deep seafloor (using 10 MPa/km of seawater, and 30 MPa/km of rock). For a 3000-m-deep seafloor, the corresponding depth is 2.0 to 2.3 km.

This treatment, using fluid inclusion and independent temperature constraints, is the only geobarometric technique that can be applied to the rocks in Hole 735B. The results, although very preliminary, confirm that the setting of this 500-m section is very near the top of layer 3 of a "normal" oceanic crust.

SUMMARY AND CONCLUSIONS

1. Hole 735B provides us with a unique view into oceanic layer 3 and allows us to examine 500 m of continuously cored material for evidence of fluid interaction. Samples are not biased toward fault scarp and talus material, as is unfortunately true of dredged and submersible-sampled rocks. One must remember, however, that Hole 735B represents only a portion of layer 3 in a particular, albeit important and widespread, tectonic setting.

2. We have described and contrasted the alteration styles of four lithologies from Hole 735B: veined metagabbro, veined mylonitic gabbro, trondhjemite, and leucocratic diopside-bearing veins. Much of the alteration in Units I and II is present as early, high-temperature hornblende-andesine veins oriented perpendicular to foliation. In contrast, veining in Units III, V, VI, and the base of Unit II includes widely spaced, steeply dipping leucocratic veins, about 1 cm wide which contain diopside and plagioclase. Breccia horizons occur at irregular intervals within Units IV, V, VI, and at the Unit II/III boundary.

Most gabbros (including mylonitic ones) and trondhjemite contain evidence for the initial presence of magmatic fluids, in the form of accessory hastingsitic amphibole and chlorine- and fluorine-bearing mica, respectively. These gabbros and leucocratic veins contain evidence for further alteration by seawater-derived fluids at variable temperature and water/rock ratio.

3. Amphiboles are dominated by hornblendes, with tremolite, actinolite, and cummingtonite also present. Hornblendes vary from high-aluminum sodic varieties (hastingsitic or pargasitic), generally confined to early petrographic modes, through magnesio-hornblendes forming much of the metamorphic/hydrothermal vein amphibole, to low-aluminum retrograde actinolitic hornblende and actinolite. Many samples contain a continuous range of these hornblende compositions. Oscillatory zonation of some late-stage hornblende shows that some fluid composition and physical parameters fluctuated repeatedly.

4. Chlorine concentration is low in early high-temperature hastingsitic/pargasitic hornblendes and in late low-aluminum actinolitic hornblendes and actinolite, but is significant in many magnesio-hornblendes, reaching about 1.5 wt%. This is

particularly true for metagabbros from Units I and II. We interpret the chlorine concentration in hornblende to reflect interaction of the gabbros with seawater, with particularly low water/rock ratios in Units I and II.

5. Analyzed feldspars range from igneous labradorite to albite. In Units I and II, labradorite has been commonly altered at the grain edges and cut by veinlets of andesine. In Units III, V, VI, and the base of Unit II, similar veinlets are andesine and oligoclase, with some samples exhibiting development of late-stage albite. Orthoclase content of plagioclase reaches about 2 mol%, with one sample containing up to 7 mol% orthoclase component in albite within a small shear zone.

6. A level near Core 118-735B-30R marks a boundary between two contrasting alteration styles. Above Core 118-735B-30R, rocks are highly strained in a pervasive, ductile fashion, with early high-temperature veining. The vein compositions (mineral and isotopic) suggest that seawater was involved throughout, at high temperature (of the order of 600°C) and low water/rock ratio. Core 118-735B-30R marks the approximate upper limit of diopside-bearing veins and alteration assemblages containing epidote and titanite. Below Core 118-735B-30R, alteration occurred at more discrete zones of veining or brecciation, continued to lower temperatures, and was accompanied by seawater-derived fluids. Within veins, the local water-rock ratio was high, although integrated over the whole lower part of the drill hole, the water/rock ratio was low.

7. Fluid inclusions are abundant in metagabbro (plagioclase and hornblende are the host phases), trondhjemite (within plagioclase and quartz), and leucocratic veins (within plagioclase and diopside).

Many fluid inclusions within metagabbro plagioclase and within trondhjemite quartz contain a methane-water fluid of low salinity. No other gases were detected. These inclusions are interpreted as early secondary inclusions, associated with the andesine-hornblende alteration in gabbro and with the trondhjemite intrusion. The fluid has a seawater origin.

Fluid inclusions in diopside from the leucocratic diopside-bearing veins contain low-salinity, gas-free inclusions of seawater origin. Plagioclase interstitial to the diopside contains inclusions with a lower-salinity, lower-temperature fluid, reflecting continued plagioclase recrystallization under retrograde conditions.

8. Oxygen isotope ratios were analyzed on mineral separates. Igneous augites retained their primary isotopic signature, but coexisting plagioclase in metagabbros and mylonitic metagabbros have been isotopically depleted to varying degrees. This depletion of plagioclase is a sensitive and diagnostic indicator of seawater-rock interaction. In the mylonitic metagabbro, slight depletion in plagioclase suggests a low water/rock ratio. In some altered metagabbros, more thorough exchange in the plagioclase was observed, suggesting that the water/rock ratio was higher (probably much greater than one).

Isotopically heavy values for plagioclase in some leucocratic veins, approaching expected igneous values, supports the hypothesis that some of these veins and associated breccia horizons were filled by a late magmatic, trondhjemitic liquid (see Stakes et al., this volume). However, the plagioclase separates from the two heaviest samples have been contaminated by isotopically heavy prehnite or analcime, which complicates the interpretation.

Leucocratic diopside-bearing veins contain isotopically light plagioclase and diopside that has been interpreted as of seawater-related hydrothermal origin.

9. Seawater was the origin of most fluids that altered rocks from Hole 735B, based on oxygen isotopic, mineral chemical, and fluid inclusion data. The methane in many fluid inclusions may have had one of several possible origins: (1) methane could be a magmatic gas, although mid-ocean ridge basalts presumably are accompanied by carbon dioxide and water, with only minor methane; (2) primitive mantle methane could have leaked up into layer 3, but even mantle fluids are thought to be dominated by carbon dioxide and water, with up to about 10% methane; (3) methane may be a by-product of serpentinization reactions, either within upper mantle or cumulate ultramafic rocks, or possibly even within layer 3 itself (for example, in Units I and II, where hydration of mafic phases took place under low water/rock conditions); (4) biogenic methane may have entered a seafloor hydrothermal system, although this is unlikely to be the source of the methane observed in layer 3.

10. Hornblende-plagioclase and isotopic temperatures determined for Hole 735B range from 720°C (early development of hornblende and andesine in metagabbro) through 500° to 600°C (the majority of hornblende-intermediate plagioclase veining), to temperatures below 400°C (retrograde development of greenschist-type assemblages including titanite, epidote, and prehnite; and even later development of analcime and thomsonite). A temperature for a leucocratic diopside-bearing vein, based on plagioclase-amphibole equilibria and consistent with oxygen isotopic modeling of diopside and plagioclase, was estimated as 500° ± about 20°C.

11. The combination of fluid inclusion data and geothermometry allows one to determine a pressure for a diopside-bearing vein sample. The primary inclusions homogenize at 410° ± 10°C, and the minerals formed at around 500°C. The pressure that rectifies these two determinations is 90 to 100 MPa (900–1000 bars). Assuming a lithostatic load and a 4000-m-deep ridge crest, this pressure range corresponds to a depth of 1.7 to 2.0 km (or, 2.0–2.3 km below a 3000-m-deep ridge crest). Consequently, the gabbroic section sampled at Hole 735B was formed at a mid-ocean ridge crest at a depth just below the extrusive carapace and an intervening sheeted dike section, assuming current seismic and ophiolite-based models of ocean crustal structure are applicable to the Southwest Indian Ridge.

ACKNOWLEDGMENTS

This work was supported by the NSF (OCE-8710717, OCE-8906261 to DAV; OCE-8902586 to DSS) and JOI-USSAC (Texas A&M FD20195 to DSS). We are grateful to Sean Heinzquith for preparing the doubly polished rock sections and for collecting some of the fluid inclusion measurements; to Kyle Kirschenmann and Leon Ember for obtaining the oxygen isotopic data; to Janice Crosby, Teresa Chaput, Steve Stonehill, and Mian Hong, who assisted with the arduous task of mineral separations; to Scott Vetter for assistance with electron microprobe analyses; and to Bob Bodnar and Cheryl Knight from the Vibrational Spectroscopy Laboratory at Virginia Tech for aid in obtaining laser Raman microprobe analyses. Stan Hart provided unpublished Sr isotope results on vein calcite. Two anonymous reviewers provided substantial help in improving the manuscript; we also acknowledge helpful discussions with Henry Dick, Jim Natland, Catherine Mevel, Mathilde Cannat, Jeff Alt, and Devamoni Naidoo.

REFERENCES

- Abrajano, T. A., Sturchio, N. C., Bohlke, J. K., Lyon, G. L., Poreda, R. J., and Stevens, C. M., 1988. Methane-hydrogen gas seeps, Zambales ophiolite, Philippines: deep or shallow origin? *Chem. Geol.*, 71:211–222.
- Batiza, R., and Vanko, D. A., 1985. Petrologic evolution of large failed rifts in the Eastern Pacific: Petrology of volcanic and plutonic rocks from the Mathematician Ridge area and the Guadalupe Trough. *J. Petrol.*, 26:564–602.
- Bird, D. K., Rogers, R. D., and Manning, C. E., 1986. Mineralized fracture systems of the Skaergaard intrusion, East Greenland. *Meddelelser om Gronland, Geosci.*, 16:3–68.
- Bird, D. K., Schiffman, P., Elders, W. A., Williams, A. E., and McDowell, S. D., 1984. Calc-silicate mineralization in active geothermal systems. *Econ. Geol.*, 79:671–695.
- Byers, C. D., Garcia, M. O., and Muenow, D. W., 1986. Volatiles in basaltic glasses from the East Pacific Rise at 21°N: implications for MORB sources and submarine lava flow morphology. *Earth Planet. Sci. Lett.*, 76:9–20.
- Byers, C. D., Muenow, D. W., and Garcia, M. O., 1983. Volatiles in basalts and andesites from the Galapagos Spreading Center, 85° to 86°W. *Geochim. Cosmochim. Acta*, 47:1551–1558.
- Christie, D. M., Carmichael, I.S.E., and Langmuir, C. H., 1986. Oxidation states of mid-ocean ridge basalt glasses. *Earth Planet. Sci. Lett.*, 79:397–411.
- Clayton, R. N., and Mayeda, T. K., 1963. The use of bromine pentafluoride in the extraction of oxygen from oxides and silicates for isotopic analysis. *Geochim. Cosmochim. Acta*, 27:43–52.
- Deer, W. A., Howie, R. A., and Zussman, J., 1966. *An Introduction to the Rock-Forming Minerals*: London (Longman).
- Delaney, J. R., Muenow, D. W., and Graham, D. G., 1978. Abundance and distribution of water, carbon and sulfur in the glassy rims of submarine pillow basalts. *Geochim. Cosmochim. Acta*, 42:581–594.
- Frost, B. R., 1985. On the stability of sulfides, oxides, and native metals in serpentinite. *J. Petrol.*, 26:31–63.
- Goldfarb, M. S., and Delaney, J. R., 1988. Response of two-phase fluids to fracture configurations within submarine hydrothermal systems. *J. Geophys. Res.*, 93:4585–4594.
- Gregory, R. T., and Taylor, H. P., Jr., 1981. An oxygen isotope profile in a section of Cretaceous oceanic crust, Samail ophiolite, Oman: Evidence for ¹⁸O buffering of the oceans by deep (>5 km) seawater-hydrothermal circulation at mid-ocean ridges. *J. Geophys. Res.*, 86:2737–2755.
- Harper, G. D., Bowman, J. R., and Kuhns, R., 1988. A field, chemical, and stable isotope study of seafloor metamorphism of the Josephine Ophiolite, California-Oregon. *J. Geophys. Res.*, 93:4625–4656.
- Ito, E., and Anderson, A. T., Jr., 1983. Submarine metamorphism of gabbros from the Mid-Cayman Rise: petrographic and mineral constraints on hydrothermal processes at slow-spreading ridges. *Contrib. Mineral. Petrol.*, 82:371–388.
- Ito, E., and Clayton, R. N., 1983. Submarine metamorphism of gabbros from the Mid-Cayman Rise: an oxygen isotopic study. *Geochim. Cosmochim. Acta*, 47:535–546.
- Janecky, D. R., and Seyfried, W. E., Jr., 1986. Hydrothermal serpentinization of peridotite within the oceanic crust: experimental investigations of mineralogy and major element chemistry. *Geochim. Cosmochim. Acta*, 50:1357–1378.
- Kelley, D. S., and Delaney, J. R., 1987. Two-phase separation and fracturing in mid-ocean ridge gabbros at temperatures greater than 700°C. *Earth Planet. Sci. Lett.*, 83:53–66.
- Leake, B. E., 1978. Nomenclature of amphiboles. *Canad. Mineral.*, 16:501–520.
- Liou, J. G., Kuniyoshi, S., and Ito, K., 1974. Experimental studies of the phase relations between greenschist and amphibolite in a basaltic system. *Am. J. Sci.*, 274:613–632.
- Liou, J. G., Kim, H. S., and Maruyama, S., 1983. Prehnite-epidote equilibria and their petrologic applications. *J. Petrol.*, 24:321–342.
- Malcolm, F. L., 1981. Microstructures of the Cayman Trough gabbros. *J. Geol.*, 89:675–688.

- Maruyama, S., Suzuki, K., and Liou, J. G., 1983. Greenschist amphibolite transition equilibria at low pressure. *J. Petrol.*, 24:583–604.
- Mathews, A., Goldsmith, J. R., and Clayton, R. N., 1983. Oxygen isotope fractionations involving pyroxenes: the calibration of mineral-pair geothermometers. *Geochim. Cosmochim. Acta*, 47:631–644.
- Mevel, C., 1988. Metamorphism in oceanic layer 3, Gorrige Bank, Eastern Atlantic. *Contrib. Mineral. Petrol.*, 100:496–509.
- Moody, J. B., Meyer, D., and Jenkins, J. E., 1983. Experimental characterization of the greenschist/amphibolite boundary in mafic systems. *Am. J. Sci.*, 283:48–92.
- Mottl, M. J., 1983. Metabasalts, axial hot springs, and the structure of hydrothermal systems at mid-ocean ridges. *Geol. Soc. Am. Bull.*, 94:161–180.
- Muenow, D. W., Liu, N. W. K., Garcia, M. O., and Saunders, A. D., 1980. Volatiles in submarine volcanic rocks from the spreading axis of the East Scotia Sea back-arc basin. *Earth Planet. Sci. Lett.*, 47:272–278.
- Mullis, J., 1979. The system methane-water as a geologic thermometer and barometer from the external part of the Central Alps. *Bull. Mineral.*, 102:526–536.
- O'Neil, J. R., and Taylor, H. P., Jr., 1967. The oxygen isotope and cation exchange chemistry of feldspars. *Am. Mineral.*, 52:1414–1437.
- Plyusnina, L. P., 1982. Geothermometry and geobarometry of plagioclase-hornblende bearing assemblages. *Contrib. Mineral. Petrol.*, 80:140–146.
- Prichard, H. M., and Cann, J. R., 1982. Petrology and mineralogy of dredged gabbro from Gettysburg Bank, Eastern Atlantic. *Contrib. Mineral. Petrol.*, 79:46–55.
- Robinson, P., Spear, F. S., Schumacher, J. C., Laird, J., Klein, C., Evans, B. W., and Doolan, B. L., 1982. Phase relations of metamorphic amphiboles: natural occurrence and theory. In Veblen, D. R., and Ribbe, P. H. (Eds.), *Amphiboles: Petrology and Experimental Phase Relations: Rev. Mineral. 9B*: Washington (Mineral. Soc. Am.), 1–227.
- Roedder, E., 1984. *Fluid Inclusions: Rev. Mineral. 12*: Washington (Mineral. Soc. Am.).
- Roedder, E., and Bodnar, R. J., 1980. Geologic pressure determinations from fluid inclusion studies. *Annu. Rev. Earth. Planet. Sci.*, 8:263–301.
- Schiffries, C. M., 1985. Reconnaissance study of fluid inclusions in the Bushveld Complex. *EOS Trans. Am. Geophys. Union*, 66:418. (Abstract)
- Schiffries, C. M., and Rye, D. M., 1990. Stable isotopic systematics of the Bushveld Complex: II. Constraints on hydrothermal processes in layered intrusions. *Am. J. Sci.*, 290:209–245.
- Schiffries, C. M., and Skinner, B. J., 1987. The Bushveld hydrothermal system: field and petrologic evidence. *Am. J. Sci.*, 287:566–595.
- Shipboard Scientific Party, 1989. Site 735. In Robinson, P. T., Von Herzen, R., et al., *Proc. ODP, Init. Repts.*, 118: College Station, TX (Ocean Drilling Program), 89–222.
- Spear, F. S., 1980. NaSi \rightleftharpoons CaAl exchange equilibrium between plagioclase and amphibole: an empirical model. *Contrib. Mineral. Petrol.*, 72:33–41.
- Stakes, D. S., and O'Neil, J. R., 1982. Mineralogy and stable isotope geochemistry of hydrothermally altered oceanic rocks. *Earth Planet. Sci. Lett.*, 57:285–304.
- Stakes, D. S., and Vanko, D. A., 1986. Multistage hydrothermal alteration of gabbroic rocks from the failed Mathematician Ridge. *Earth Planet. Sci. Lett.*, 79:75–92.
- Taylor, H. P., Jr., 1968. The oxygen isotope geochemistry of igneous rocks. *Contrib. Mineral. Petrol.*, 19:1–71.
- Taylor, H. P., Jr., 1977. Water/rock interactions and the origin of H₂O in granitic batholiths. *J. Geol. Soc. (London)*, 133:509–558.
- Vanko, D. A., 1986. High-chlorine amphiboles from oceanic rocks: product of highly-saline hydrothermal fluids? *Am. Mineral.*, 71:51–59.
- Vanko, David A., 1988. Temperature, pressure, and composition of hydrothermal fluids, with their bearing on the magnitude of tectonic uplift at mid-ocean ridges, inferred from fluid inclusions in oceanic layer 3 rocks. *J. Geophys. Res.*, 93:4595–4611.
- Vanko, D. A., and Batiza, R., 1982. Gabbroic rocks from the Mathematician Ridge failed rift. *Nature*, 300:742–744.
- Welhan, J. A., 1988. Origins of methane in hydrothermal systems. *Chem. Geol.*, 71:183–198.
- Welhan, J. A., and Craig, H., 1983. Methane, hydrogen and helium in hydrothermal fluids at 21°N on the East Pacific Rise. In Rona, P. A., Bostrom, K., Laubier, L., and Smith, K. L., Jr. (Eds.), *Hydrothermal Processes at Seafloor Spreading Centers*: New York (Plenum), 391–409.
- Wood, B. J., and Virgo, D., 1989. Upper mantle oxidation state: ferric iron contents of ilmenite spinels by ⁵⁷Fe Mossbauer spectroscopy and resultant oxygen fugacities. *Geochim. Cosmochim. Acta*, 53:1277–1291.
- Wopenka, B., and Pasteris, J. D., 1987. Raman intensities and detection limits of geochemically relevant gas mixtures for a laser Raman microprobe. *Analytical Chem.*, 59:2165–2170.
- Wopenka, B., Pasteris, J. D., and Freeman, J. J., in press. Analysis of individual fluid inclusions by FTIR and Raman micro-spectroscopy. *Geochim. Cosmochim. Acta*, 54.

Date of initial receipt: 17 July 1989

Date of acceptance: 22 May 1990

Ms 118B-121

APPENDIX

Sample Descriptions

Veined Metagabbros

Sample 118-735B-22R-3 (Piece 5A, 112–115 cm) is a Unit II gabbro with primary gabbroic texture cut by a network of amphibole veinlets. The bulk of the rock is gabbroic, with equant plagioclase crystals; intergranular to oikocrystic clinopyroxenes that are altered at the edges to coronitic layers of tremolite, cummingtonite, and actinolite; and small serpentine plus opaque pseudomorphs of olivine that are enclosed in pyroxene. Parts of the gabbro are coarse, with typical 6-mm-diameter grains, and other parts of the sample are finer grained (1-mm grains). Cutting this mildly hydrated gabbro are millimeter-scale veins of an amphibole that is pleochroic from light green to tan. In the immediate vicinity of the amphibole veins, the host gabbro is more heavily altered, with amphibole replacing clinopyroxene and igneous plagioclase veined by tiny sodic plagioclase veins. The plagioclase in this sample is labradorite with secondary oligoclase, and the secondary amphibole is magnesio-hornblende.

Sample 118-735B-25R-1 (Piece 3, 12–17 cm) from Unit II is a deformed metagabbro exhibiting locally both areas of foliated gabbroic texture and areas of cataclastic texture featuring a drastic grain-size reduction. In the foliated, porphyroclastic sections, grains measure up to 5 mm across, whereas the cataclastic sections have sub-millimeter grains. This metagabbro is essentially a plagioclase-amphibole rock, with relict clinopyroxene enclosed in amphibole porphyroclasts. The amphibole is mostly green, but also contains irregular brown zones, and it contains inclusions of ilmenite and pyrite. Plagioclase is an igneous labradorite and is characterized by the presence of abundant tiny (sub-micrometer to micrometer-scale) opaque inclusions that are rods and flakes, oriented with respect to the enclosing plagioclase crystal. These opaque inclusions give the plagioclase a turbid appearance and have been noted in many other oceanic plutonic plagioclases (e.g., Batiza and Vanko, 1985). Plagioclase in this sample is altered around grain edges and along grain-cutting veinlets (5–150 μ m wide) to oligoclase, which is characterized by the absence of opaque oriented inclusions. By contrast the oligoclase contains abundant fluid inclusions. Amphibole locally forms sharp-edged veinlets, 40 to 200 μ m wide, cutting the plagioclase at a high angle to the rock's foliation (Fig. 3). This amphibole appears to be an extension of the amphibole in porphyroclasts. It is classified as magnesio-hornblende, with some actinolitic hornblende.

Sample 118-735B-26R-2 (Piece 2A, 8–12 cm) is another Unit II metagabbro with a net of amphibole veins. Labradorite grains 0.5 to 1 mm wide and relict clinopyroxene porphyroclasts up to 10 mm wide are the primary igneous phases. Pyroxene has an amphibole (uralite) rim extending and blending with the amphibole in the veins, which is granular and up to 2 mm across. The amphibole is green, but is zoned in an oscillatory fashion through various shades of blue-green and clear where euhedral blades appear to have grown into tiny vugs (Fig. 4). The amphibole is magnesio-hornblende zoned to actinolite. Sec-

ondary plagioclase forms along igneous plagioclase edges and as tiny cross-cutting veins (Fig. 5). This plagioclase is andesine and contains abundant aqueous fluid inclusions (Fig. 6).

Sample 118-735B-58R-1 (Piece 10, 47–51 cm) is a metagabbro from near the top of Unit V, located less than 7 m from the major shear zone or fault zone separating Units IV and V. It is heavily altered, with relict igneous plagioclase (labradorite) and clinopyroxene measuring up to 6 mm wide. In addition to its calcic composition, igneous plagioclase is readily recognized because of its dense packing with tiny oriented opaque inclusions. Abundant secondary plagioclase (oligoclase through albite) has replaced the igneous plagioclase, along with prehnite, clinozoisite, thomsonite, and calcite. Other secondary phases are titanite, traces of diopside, and tremolite/actinolite coronitic pseudomorphs of a preexisting mafic phase. Plagioclase in this sample contains abundant fluid inclusions, some measuring up to 100 μm (Figs. 7, 8).

Veined mylonitic gabbro

Sample 118-735B-2D-2 (Piece 6, 36–39 cm) is a representative example from Unit I. Plagioclase (labradorite) and clinopyroxene (augite) form porphyroclasts up to 4 mm across. Mosaic plagioclase (typically 200 μm and less) and pyroxene form a banded foliation. Also contributing to the foliation are stretched patches of fine-medium cummingtonite surrounded by green actinolite, probably resulting from hydration of orthopyroxene and/or olivine. Small amounts of brown amphibole (magnesian-hastingsite) occur as islands within pyroxene porphyroclasts and in pressure shadows or tails on those porphyroclasts. Cutting this mylonitic gabbro at a high angle is a green amphibole (magnesian-hornblende) vein, with minor plagioclase and trace apatite. Clinopyroxene porphyroclasts immediately adjacent to the vein are partially uralitized to green hornblende.

Trondhjemite

Sample 118-735B-54R-2 (Piece 1C, 32–34 cm) contains trondhjemite and partially absorbed relict xenocrysts of plagioclase, clinopyroxene, and mafic clots. The plagioclase (andesine) porphyroclasts are cut by veinlets of oligoclase and albite. Pyroxenes are altered at the edge to amphibole, and mafic clots consist of concentric zones ranging from fine-grained phyllosilicate stained with iron oxyhydroxide at the core, to cummingtonite, to forest green ferrohornblende through ferroactinolite. The bulk of the rock, however, is a medium-grained plagioclase-quartz rock, containing blocky tablets of oligoclase through albite, anhedral quartz, and interstitial trace amounts of biotite, apatite, and pyrite. Much of the quartz and plagioclase is intergrown in graphic or granophyric textures (Fig. 9). Scant fluid inclusions are present within quartz (Fig. 10) and plagioclase.

Leucocratic Diopside-Bearing Veins

Sample 118-735B-70R-1 (Piece 2B, 39–49 cm) is an extremely fresh medium-grained (typical 4-mm grains) two-pyroxene gabbro cut by a leucocratic vein. The vein has a color index of about 50 and contains plagioclase (albite to oligoclase) and diopside, with accessory pink titanite, clinozoisite, and chlorite. Plagioclase in the host rock is labradorite. Beyond the vein edges, there is very little alteration of the host gabbro: a few small veinlets of sodic plagioclase cut through adjacent labradorite crystals.

This leucocratic vein is straight- and sharp-edged, a constant 8 mm wide, but a 1-mm apophysis extends at low angle from one side of the vein. The vein texture mimics the gabbroic texture of the host rock (Fig. 12). The diopside and oligoclase form a medium-grained gabbroic texture similar to that of the fresh host rock. In addition, diopside forms a crystallographically aligned continuation of fresh host-rock augite, and oligoclase forms adjacent to host-rock labradorite (Fig. 12). The diopside and oligoclase within the vein contain abundant fluid inclusions (Fig. 11).

Sample 118-735B-63R-6 (Piece 5A, 94–98 cm) contains a steeply dipping leucocratic vein cutting a Unit V gabbro. The vein is 8 mm wide, but its edges are somewhat gradational. The color index of this vein is low (<5), while plagioclase (oligoclase to andesine) is the dominant mineral. Diopside comprises <5% of the vein, and accessory minerals include clinozoisite, titanite, and chlorite. The host gabbro contains labradorite, augite, and alteration pseudomorphs of olivine. On one side of the vein, the host gabbro is heavily veined by sodic plagioclase, and on the other side the gabbro is full of tiny calcite veinlets. This vein does not exhibit epitaxial growth of diopside on augite. The diopside and plagioclase contain abundant fluid inclusions.

Sample 118-735B-40R-3 (Piece 3A, 34–39 cm) is a coarse Unit III metagabbro containing a diopside-bearing leucocratic vein-like zone whose mineralogy is dominantly plagioclase-diopside, with accessory amphibole and clinozoisite. The diopside contains abundant fluid inclusions.

Sample 118-735B-81R-2 (Piece 1C, 23–31 cm) is a Unit VI gabbro with a leucocratic zone devoid of diopside. The host contains coarse (2–10 mm) labradorite, augite (typically 6 mm), rounded olivine (1–2 mm), and mild hydration products (uralite on pyroxene; iddingsite, tremolite and cummingtonite on olivine). Cutting diffusely through the gabbro is a zone of alteration, where plagioclase (albite) is the major mineral. Accessories include actinolite and ferroactinolite in clots, apatite (up to 0.5 mm), trace ilmenite, pink titanite (probably containing rare earth or other trace elements), euhedral zircon (up to 0.8 mm wide), and rare quartz (0.5 mm across). Fluid inclusions are present in both quartz and albite.